

# 1 Technical Note: Nighttime OH and HO<sub>2</sub> chemical equilibria in the mesosphere – lower 2 thermosphere

3 Mikhail Yu. Kulikov<sup>1</sup>, Mikhail V. Belikovich<sup>1</sup>, Aleksey G. Chubarov<sup>1</sup>, Svetlana O. Dementyeva<sup>1</sup>, and  
4 Alexander M. Feigin<sup>1</sup>

5 <sup>1</sup>A. V. Gaponov-Grekhov Institute of Applied Physics of the Russian Academy of Sciences, 46 Ulyanov  
6 Str., 603950 Nizhny Novgorod, Russia

7 Correspondence to: Mikhail Yu. Kulikov (mikhail\_kulikov@mail.ru)

8  
9 **Abstract.** At the altitudes of the mesosphere – lower thermosphere, OH and HO<sub>2</sub> play a significant  
10 role in many physicochemical processes. Thus, monitoring ~~of~~ their spatiotemporal evolution together with  
11 other chemically active trace gases is one of the most important problems for this atmosphere region, in  
12 which direct measurements are difficult. The paper studies the nighttime OH and HO<sub>2</sub> chemical equilibria  
13 using the 3D chemical transport modeling within the general approach ~~including, which includes~~ the  
14 ~~extraction~~ identification of the main sources and sinks in the equilibrium space-time areas and derivation  
15 of analytical criteria for equilibrium validity. The presented analysis shows, ~~that~~ there are extended areas,  
16 where nighttime HO<sub>2</sub> and OH are close to their local equilibrium concentrations, ~~determined~~ determined mainly by  
17 the reaction between HO<sub>x</sub> – O<sub>x</sub> components among themselves and with H<sub>2</sub>O<sub>2</sub>, N, NO, NO<sub>2</sub>, and CO. In  
18 the upper mesosphere – lower thermosphere, the equilibrium expressions can be shortened, including so  
19 that they include the HO<sub>x</sub> – O<sub>x</sub> chemistry only. These ~~conditions describe~~ expressions describe the HO<sub>2</sub>  
20 and OH ~~equilibrium~~ equilibria from the top down to ~~the~~ some ~~lower borders~~ boundaries, the altitude  
21 ~~position~~ positions of which vary in the interval between 72-73 and 85 km and ~~depends~~ depend essentially  
22 on season and latitude. The developed analytical criteria almost everywhere ~~well~~ reproduce well the main  
23 features of these ~~borders~~ boundaries. Due to weak sensitivity to uncertainties of reaction rates and other  
24 parameters, the criteria can be considered a robust instrument for HO<sub>2</sub> and OH equilibrium validation.  
25 The obtained results allow us to extend ~~the abilities of~~ previously proposed methods for the retrieval of  
26 poorly measured components from measurement data and to develop new approaches.

## 28 1 Introduction

29 Monitoring the spatiotemporal evolution of chemically active trace gases is one of the most  
30 important problems in atmospheric research. Despite the increase of the experimental data volume  
31 nowadays, primarily due to the development ~~of~~ remote sensing methods, many important trace gases  
32 continue to be unavailable for direct and regular measurements. A well-known way to increase the  
33 information content of experimental campaigns is to use ~~chemical transport models and~~ the available  
34 experimental data ~~for deriving~~ in conjunction with a certain chemical or physicochemical model to derive  
35 unmeasured characteristics indirectly. Within the framework of this approach, the model acts as *a priori*  
36 relationship between directly measured and retrieved characteristics. The simplest model, that makes it  
37 possible to implement this approach, is based on the condition of local (in both time and space)  
38 photochemical/chemical balance (local equilibrium) between sources and sinks of the so-called “fast”  
39 components: trace gases with short lifetimes relatively, in particular, to the characteristic transport times.  
40 Mathematically, this condition does not mean that the fast variables are at equilibrium, but when it is  
41 fulfilled, the corresponding concentrations are close to their instantaneous equilibrium values. At the  
42 same time, due to the strong dissipation, in most cases (except the special cases where the ensemble of  
43 fast components includes the slow family of these components), there is no need to follow the law of  
44 matter conservation. It is possible to ~~disregard~~ insignificant sinks and sources, including those  
45 caused by transport, in the corresponding balance equations without the loss of accuracy, ~~including those~~  
46 ~~caused by transport~~. The resulting algebraic equations are the simplest *a priori* local relations between  
47 measurable and retrieved trace gases. These relationships can be used to derive information about hard-to-  
48 measure atmospheric species, determine key atmospheric characteristics (for example, temperature),  
49 (Marchand et al., 2007), validate the data quality of simultaneous measurements of several atmospheric  
50 components, (Kulikov et al., 2018a), estimate reaction rate constants ~~known with high~~  
51 ~~uncertainty~~, (Stedman et al., 1975; Avallone and Toohey, 2001), evaluate sources ~~(emissions/sinks~~  
52 (Cantrell et al., 2003), etc.

53 For several decades, the photochemical/chemical equilibrium approximation ~~have~~ has been used to  
54 solve many atmospheric tasks. It is applied (see, e.g., the short review in Kulikov et al. (2018a) and  
55 references therein) in investigations of the surface layer and free troposphere chemistry in different  
56 regions (over ~~megalopolises~~ megapolises, in rural areas, in the mountains, over the seas), in stratospheric  
57 chemistry studies, including derivation of ~~a~~ critical parameters ~~of~~ the ozone destruction catalytic cycles,  
58 ~~to study~~ in studies of the HO<sub>x</sub> – O<sub>x</sub> chemistry and airglows (O(<sup>1</sup>S) green-line, O<sub>2</sub> A-band, OH Meinel  
59 band emissions) at the heights of the mesosphere – lower thermosphere. In the latter case, the  
60 distributions of unmeasured characteristics are determined from the data of daytime and nighttime rocket  
61 and satellite measurements (e.g., Evans and Llewellyn, 1973; Good, 1976; Pendleton et al., 1983;

62 McDade et al., 1985; McDade and Llewellyn, 1988; Evans et al., 1988; Thomas, 1990; Llewellyn et al.,  
63 1993; Llewellyn and McDade, 1996; Russell and Lowe, 2003; Russell et al., 2005; Kulikov et al., 2006,  
64 2009, 2017, 2022a, 2022b; Mlynczak et al., 2007, 2013a, 2013b, 2014, 2018; Smith et al., 2010; Xu et al.,  
65 2012; Siskind et al., 2008, 2015; Fytterer et al., 2019) with the use of equilibrium assumptions for ozone  
66 and excited states of OH, O, and O<sub>2</sub>. For example, such an approach is applied to the data of the SABER  
67 (Sounding of the Atmosphere using Broadband Emission Radiometry) instrument onboard the TIMED  
68 (Thermosphere Ionosphere Mesosphere Energetics and Dynamics) satellite, which since 2002 continues  
69 to measure simultaneous profiles of temperature, ozone, and volume emission rates of OH\* transitions in  
70 wide ranges of altitude, local time, and latitude with a rather high space-time resolution.

71 Note a number of general aspects of the application of equilibrium conditions in the above  
72 examples. First of all, there are no clear criteria ~~why, indicating~~ the conditions under which the use of  
73 equilibrium condition should be satisfied; approximation is justified. Usually, a certain component is taken  
74 to be a fast variable, if its lifetime is much shorter, than the lifetimes of other components of studied  
75 photochemical/chemical system or the duration of a day, daytime, nighttime, etc. For example, in the  
76 papers on SABER data processing (Mlynczak et al., 2013a, 2013b, 2014, 2018), it is assumed, that the  
77 nighttime ozone chemical equilibrium in the mesopause is well fulfilled at altitudes of 80–100 km, since  
78 the nighttime ozone lifetime at these altitudes ~~is too short varying~~ varies in the range from several minutes  
79 to several tens of minutes. Note, that this assumption is quite popular and used in different tasks (e.g.,  
80 Swenson and Gardner, 1998; Marsh et al., 2006; Smith et al., 2009; Nikoukar et al., 2007; Xu et al., 2010,  
81 2012; Kowalewski et al., 2014; Grygalashvyly et al., 2014; Grygalashvyly, 2015; Sonnemann et al., 2015;  
82 Kulikov et al., 2021). Belikovich et al. (2018) and Kulikov et al. (2018b, 2019, 2023a) analyzed the  
83 nighttime ozone chemical equilibrium numerically, analytically, and with the use of SABER/TIMED  
84 data. It was revealed, that the short lifetime is not a sufficient condition, so, this equilibrium may be  
85 significantly ~~disrupted~~ disturbed above 80 km. ~~Secondly, there is no detailed numerical examination of~~  
86 ~~this approximation validity, depending on altitude, latitude,~~ The local time ratio between true and season-  
87 Correspondingly, there is no equilibrium concentrations may vary widely and reach up to several orders of  
88 magnitude (e.g., Figure 5 in Kulikov et al. (2018b)). Thus, without special restrictions the assessment of  
89 possible error ~~error~~ in retrieved characteristics due to ~~disturbance of the used equilibrium condition~~  
90 the use of equilibrium approximation is uncontrollable and may significantly exceed all other errors in the  
91 retrieval procedure due to, for example, uncertainties in the measurement data and rate constants.

92 ~~Starting since our~~ Since the papers ~~by of~~ Belikovich et al. (2018) and Kulikov et al. (2018b, 2019,  
93 2023a), we ~~develop~~ developed the general approach to ~~correct search of~~ correctly identify fast components  
94 using, employing the data from a global 3D chemical transport model. It includes:

95 1. Plotting of the equilibrium space-time maps of ~~interested component~~ the components of interest.

- 96 2. Identification of the main sources and sinks in the found equilibrium areas.
- 97 3. Derivation and subsequent use of analytical criteria that make it possible to determine the fulfillment of
- 98 the equilibrium condition locally (in time and space) with the use of the measurement data only.

99 The ~~lastlatter~~ point is based on the theory of chemical equilibrium of a certain trace gas ~~based on,~~  
100 ~~acquired from~~ estimations of its lifetime and equilibrium concentration, and time dependences of these  
101 characteristics (Kulikov et al., 2023a). Note, that when equilibrium condition is applied to measurement  
102 data in the retrieval of unmeasured characteristics, the criterion allows controlling and limiting the  
103 possible error caused by the equilibrium approximation.

104 The main ~~goalsgoal~~ of ~~this~~the paper is to apply ~~mentioned~~this approach ~~for to the~~ analysis of  
105 nighttime OH and HO<sub>2</sub> chemical ~~equilibrium~~equilibria in the mesosphere – lower thermosphere. Along  
106 with O and H, OH and HO<sub>2</sub> are important components of HO<sub>x</sub> – O<sub>x</sub> chemistry, participating (a) in  
107 chemical heating through, in particular, O+OH → O<sub>2</sub>+H and O+HO<sub>2</sub> → O<sub>2</sub>+OH exothermic reactions, (b)  
108 in formation of airglows, (c) in catalytic cycles of the ozone destruction. Moreover, the equilibrium  
109 conditions of OH and HO<sub>2</sub> are additional *a priori* relationships, that can be used to retrieve these  
110 components or other characteristics from measured data. In particular, ~~the method proposed by~~Panka et  
111 al. (2021) ~~proposed the method~~ for nighttime total OH retrieval from SABER/TIMED data at 80-100 km,  
112 which does not use the ~~nighttime~~-ozone chemical equilibrium, ~~but nevertheless,~~ However, the method  
113 applies the equilibrium between sources and sinks for all excited and ground not only to excited states of  
114 OH (~~v=0-9~~), with ultrashort lifetimes, but also to the ground state. Therefore, this ~~approach~~point is  
115 ~~tested~~verified in our paper.

116 In the next section, we present the used model and methods. In Section 3, the model data are used to  
117 plot HO<sub>2</sub> and OH equilibrium maps. In Sections 4-5, we ~~extract~~identify the main reactions, determining  
118 equilibria of these gases, and present their shortened equilibria conditions at the upper mesosphere and  
119 lower thermosphere altitudes. In Section 6, the criteria for HO<sub>2</sub> and OH equilibria validity are developed.  
120 In Section 7, we discuss the obtained results and their possible applications.

## 122 2 Used 3D model and Approaches

123 The analysis of OH and HO<sub>2</sub> nighttime chemical equilibria was carried out, using the data, obtained  
124 with calculation of 3D chemical transport model of the middle atmosphere, developed at the Leibniz  
125 Institute of Atmospheric Physics (e.g., Sonnemann et al., 1998; Körner & Sonnemann, 2001;  
126 Grygalashvyly et al., 2009; Hartogh et al., 2004, 2011) to investigate the mesosphere – lower  
127 thermosphere chemistry, in particular, in the extended mesopause region. A number of papers (e.g.,

Hartogh et al., 2004, 2011; Sonnemann, et al., 2006, 2008) validated the model with measurements, in particular, for ozone and water vapour/vapor.

The space-time distribution of temperature and winds were taken from the model of the dynamics of the middle atmosphere COMMA-IAP (e.g., Kremp et al., 1999; Berger and von Zahn, 1999) with an updated frequency of 1 day and linear smoothing between subsequent updates to avoid unrealistic jumps in the calculated concentrations of trace gases. 3D advective transport is taken into account with the use of the Walcek-scheme (Walcek, 2000). The vertical diffusive transport (turbulent and molecular) is calculated with the use of the implicit Thomas algorithm (Morton and Mayers, 1994). The model grid includes 118 pressure-headheight levels (0–135 km), 16 latitudinal and 32 longitudinal levels. The chemical module (see Table 1) comprises 25 constituents (O, O(<sup>1</sup>D), O<sub>3</sub>, H, OH, HO<sub>2</sub>, H<sub>2</sub>O<sub>2</sub>, H<sub>2</sub>O, H<sub>2</sub>, N, NO, NO<sub>2</sub>, NO<sub>3</sub>, N<sub>2</sub>O, CH<sub>4</sub>, CH<sub>2</sub>, CH<sub>3</sub>, CH<sub>3</sub>O<sub>2</sub>, CH<sub>3</sub>O, CH<sub>2</sub>O, CHO, CO, CO<sub>2</sub>, O<sub>2</sub>, N<sub>2</sub>), 54 chemical reactions between them, and 15 photo-dissociation reactions. The model utilizes the pre-calculated dissociation rates (Kremp et al., 1999) and their dependence on the altitude and solar zenith angle.

The model was used to calculate a one-year global evolution of the above mentioned trace gases. For removing the transition regions corresponding to sunset and sunrise, we took into account these only local times when the solar zenith angle  $\geq 95^\circ$  or  $> 105^\circ$ . As a result, we find the spatiotemporal series of the  $OH/OH^{eq}$  and  $HO_2/HO_2^{eq}$  ratios. Here,  $OH$  and  $HO_2$  are the local nighttime values of hydroxyl and hydroperoxy radicals, calculated by the model,  $OH^{eq}$  and  $HO_2^{eq}$  are their local equilibrium values, corresponding to the instantaneous balance between production and loss terms, respectively. Therefore, to determine each local value of  $OH^{eq}$  and  $HO_2^{eq}$ , we used the local values of the parameters (temperature, O<sub>2</sub>, and N<sub>2</sub>) and the concentrations of other trace gases, determining local chemical sources and sinks of  $OH$  and  $HO_2$ . Then, the  $OH/OH^{eq}$  and  $HO_2/HO_2^{eq}$  series were averaged over the zonal coordinate and time during each month and were presented as height-latitude maps, depending on the month. Each map contains lines, marking the boundaries of the equilibrium areas, where the following conditions are satisfied:

$$\left\{ \begin{array}{l} |\langle OH/OH^{eq} \rangle - 1| \leq 0.1 \\ \sigma_{OH/OH^{eq}} \leq 0.1 \end{array} \right\}, \left\{ \begin{array}{l} |\langle HO_2/HO_2^{eq} \rangle - 1| \leq 0.1 \\ \sigma_{HO_2/HO_2^{eq}} \leq 0.1 \end{array} \right\}, \quad (1)$$

where the angle brackets are used to denote the values averaged in time and space,  $\sigma_{OH/OH^{eq}}$  and  $\sigma_{HO_2/HO_2^{eq}}$  are standard deviations of the  $OH/OH^{eq}$  and  $HO_2/HO_2^{eq}$  ratios from 1, respectively.

Then, we plotted spatiotemporal maps, showing the relative contribution of each reaction to a summarized source or sink at all altitudes and latitudes. These maps helped us to identify the main sources and sinks, describing the chemical equilibrium of nighttime OH and HO<sub>2</sub> in the equilibrium areas to an accuracy of better than a few percent.

160 ~~At final stage~~Finally, we obtained and verified the analytical criteria of OH and HO<sub>2</sub> nighttime  
 161 chemical equilibria according to Kulikov et al. (2023a). The paper considered the ~~poorly~~pure chemical  
 162 evolution of a certain trace gas  $n$ . ~~It was shown:~~

$$163 \frac{dn}{dt} = I_n - S_n = -\frac{1}{\tau_n} (n - n^{eq}),$$

$$164 \tau_n = \frac{n}{S_n}, n^{eq} = \frac{n \cdot I_n}{S_n}, \tag{2}$$

165 where  $t$  is time,  $I_n$  and  $S_n$  are total photochemical/chemical sources and sinks of  $n$  respectively,  $\tau_n$  is the  
 166  $n$  lifetime and  $n^{eq}$  is its equilibrium concentration, corresponding to the condition  $I_n = S_n$ . The lifetime  
 167 determines the characteristic time scale, for which  $n$  approaches  $n^{eq}$ , when  $n^{eq} = const$ . In general case  
 168  $\tau_n$  and  $n^{eq}$  are functions of time. Kulikov et al. (2023a) showed strictly mathematically, that the local  
 169 values of  $n$  and ~~its equilibrium concentration~~  $n^{eq}$  are close to each other ( $n(t) \approx n^{eq}(t)$ ), when  $\tau_n \ll$   
 170  $\tau_{n^{eq}}$ , where  ~~$\tau_n$  is the  $n$  lifetime and~~  $\tau_{n^{eq}}$  is the local time scale of  $n^{eq}$ :

$$171 \tau_{n^{eq}} \equiv \frac{n^{eq}}{|dn^{eq}/dt|}$$

$$172 \frac{n^{eq}}{|dn^{eq}/dt|} \tag{2}$$

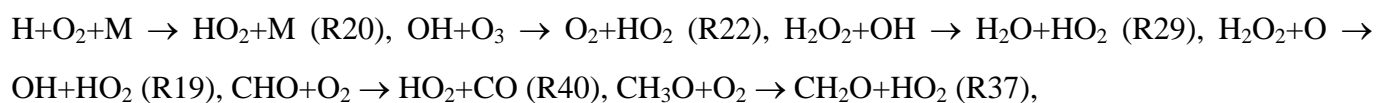
173  $\frac{n^{eq}}{|dn^{eq}/dt|} \tag{3}$   
 174 The expression for  $\tau_n$  is found from the total sink of  $n$ . The expression for  $\tau_{n^{eq}}$  is derived from Eq. (3)  
 175 with the use of differential equations, describing chemical evolution of other reacting components, which  
 176 determine the expression for  $n^{eq}$ . Kulikov et al. (2023a) also showed, when  $\tau_n \ll \tau_{n^{eq}}$ ,  $n \cong n^{eq}(1 -$   
 177  $sign(\frac{dn^{eq}}{dt}) \cdot \frac{\tau_n}{\tau_{n^{eq}}})$  in the first order approximation. Thus, the criterion

$$178 \tau_n / \tau_{n^{eq}} \leq 0.1 \tag{34}$$

179 is sufficient, in order to the possible relative difference between  $n$  and  $n^{eq}$  to be no more than 0.1.

### 181 3 Nighttime HO<sub>2</sub> and OH chemical ~~equilibrium~~equilibria

182 According to the Table 1, HO<sub>2</sub> chemical sources in nighttime are determined by the following  
 183 reactions:



186 whereas chemical sinks of this component are as follows:

187  $\text{HO}_2 + \text{O} \rightarrow \text{OH} + \text{O}_2$  (R18),  $\text{HO}_2 + \text{O}_3 \rightarrow \text{OH} + 2\text{O}_2$  (R23),  $\text{OH} + \text{HO}_2 \rightarrow \text{H}_2\text{O} + \text{O}_2$  (R28),  $\text{H} + \text{HO}_2 \rightarrow 2\text{OH}$   
 188 (R14),  $\text{H} + \text{HO}_2 \rightarrow \text{H}_2\text{O} + \text{O}$  (R15),  $\text{H} + \text{HO}_2 \rightarrow \text{H}_2 + \text{O}_2$  (R16),  $\text{NO} + \text{HO}_2 \rightarrow \text{NO}_2 + \text{OH}$  (R50),  $\text{HO}_2 + \text{HO}_2 \rightarrow$   
 189  $\text{H}_2\text{O}_2 + \text{O}_2$  (R30),  $\text{HO}_2 + \text{HO}_2 + \text{M} \rightarrow \text{H}_2\text{O}_2 + \text{O}_2 + \text{M}$  (R31).

190 Thus,  $\text{HO}_2$  local equilibrium concentration is described by the following equation:

$$191 \quad \text{HO}_2^{eq} = \frac{k_{20} \cdot \text{H} \cdot \text{M} \cdot \text{O}_2 + k_{22} \cdot \text{OH} \cdot \text{O}_3 + k_{29} \cdot \text{H}_2\text{O}_2 \cdot \text{OH} + k_{19} \cdot \text{H}_2\text{O}_2 \cdot \text{O} + k_{40} \cdot \text{CHO} \cdot \text{O}_2 + k_{37} \cdot \text{CH}_3\text{O} \cdot \text{O}_2}{k_{18} \cdot \text{O} + k_{23} \cdot \text{O}_3 + k_{28} \cdot \text{OH} + (k_{14} + k_{15} + k_{16}) \cdot \text{H} + k_{50} \cdot \text{NO} + 2 \cdot (k_{30} + k_{31}) \cdot \text{M} \cdot \text{HO}_2} \quad (45)$$

192 ~~The~~ Figure 1 plots height-latitude cross sections for the  $\langle \text{HO}_2 / \text{HO}_2^{eq} \rangle$  ratio for each month. ~~The~~  
 193 ~~dashed area corresponds to  $\chi < 95^\circ$ . The white area represents the ratio outside the [0.5, 1.5] interval.~~ The  
 194 black solid lines mark the ~~border~~boundaries of equilibrium areas, where, according to condition (1),  
 195 local values of  $\text{HO}_2$  are close to their equilibrium values with a possible bias of less than 10%. At low and  
 196 middle latitudes, one can see the ~~present~~presence of the main equilibrium area, which extends from the  
 197 top of the analyzed altitude range to the lower boundary. The height of this equilibrium ~~border~~boundary,  
 198  $z_{\text{HO}_2^{eq}}$ , depends on the season and latitude and varies in the interval between 73 and 85 km. It is the  
 199 highest and the lowest during the summer and winter respectively at the middle latitudes. Near the  
 200 equator,  $z_{\text{HO}_2^{eq}}$  demonstrates the weakest annual variations and varies in the ~~range of~~ 81-83 km range.  
 201 There are local areas below the upper longest black line, but they are small and irregular and can be  
 202 omitted from our consideration. Note ~~only~~ that the maps ~~in many months~~ show the existence of  
 203 equilibrium near 50 km, which can be assumed to be the beginning of the main equilibrium area in the  
 204 stratosphere. At high latitudes, there is the main equilibrium area as at low and middle latitudes, but this  
 205 area above  $70-75^\circ$  of latitude can extend down to 50 km ~~with small exceptions~~.

206 In accordance to the Table 1, OH chemical sources are determined by the following reactions:

207  $\text{H} + \text{O}_3 \rightarrow \text{OH} + \text{O}_2$  (R21),  $\text{HO}_2 + \text{O} \rightarrow \text{OH} + \text{O}_2$  (R18),  $\text{HO}_2 + \text{O}_3 \rightarrow \text{OH} + 2\text{O}_2$  (R23),  $\text{H} + \text{HO}_2 \rightarrow 2\text{OH}$  (R14),  
 208  $\text{NO} + \text{HO}_2 \rightarrow \text{NO}_2 + \text{OH}$  (R50),  $\text{H}_2\text{O}_2 + \text{O} \rightarrow \text{OH} + \text{HO}_2$  (R19),  $\text{H} + \text{NO}_2 \rightarrow \text{OH} + \text{NO}$  (R51),  $\text{O}(^1\text{D}) + \text{H}_2\text{O} \rightarrow$   
 209  $2\text{OH}$  (R7),  $\text{O}(^1\text{D}) + \text{H}_2 \rightarrow \text{H} + \text{OH}$  (R8),  $\text{CH}_4 + \text{O}(^1\text{D}) \rightarrow \text{CH}_3 + \text{OH}$  (R9),

210 whereas chemical sinks of this component are as follows:

211  $\text{OH} + \text{O} \rightarrow \text{H} + \text{O}_2$  (R17),  $\text{OH} + \text{O}_3 \rightarrow \text{O}_2 + \text{HO}_2$  (R22),  $\text{OH} + \text{HO}_2 \rightarrow \text{H}_2\text{O} + \text{O}_2$  (R28),  $\text{OH} + \text{OH} \rightarrow \text{H}_2\text{O} + \text{O}$   
 212 (R26),  $\text{OH} + \text{OH} + \text{M} \rightarrow \text{H}_2\text{O}_2 + \text{M}$  (R27),  $\text{H} + \text{OH} + \text{N}_2 \rightarrow \text{H}_2\text{O} + \text{N}_2$  (R24),  $\text{H}_2\text{O}_2 + \text{OH} \rightarrow \text{H}_2\text{O} + \text{HO}_2$  (R29),  
 213  $\text{OH} + \text{CO} \rightarrow \text{H} + \text{CO}_2$  (R32),  $\text{CH}_4 + \text{OH} \rightarrow \text{CH}_3 + \text{H}_2\text{O}$  (R33),  $\text{OH} + \text{H}_2 \rightarrow \text{H}_2\text{O} + \text{H}$  (R25),  $\text{N} + \text{OH} \rightarrow \text{NO} + \text{H}$   
 214 (R49).

215 Thus, OH local equilibrium concentration is described by the following equation:

$$\begin{aligned}
216 \quad OH^{eq} = & (k_{21} \cdot H \cdot O_3 + k_{18} \cdot O \cdot HO_2 + k_{23} \cdot HO_2 \cdot O_3 + 2 \cdot k_{14} \cdot H \cdot HO_2 + k_{50} \cdot HO_2 \cdot NO + k_{19} \cdot \\
217 \quad & H_2O_2 \cdot O + k_{24} \cdot H \cdot N_2 + k_{51} \cdot NO_2 \cdot H + 2 \cdot k_7 \cdot O(^1D) \cdot H_2O + k_8 \cdot O(^1D) \cdot H_2 + k_9 \cdot O(^1D) \cdot \\
218 \quad & CH_4) / (k_{17} \cdot O + k_{22} \cdot O_3 + k_{28} \cdot HO_2 + 2 \cdot (k_{26} + k_{27} \cdot M) \cdot OH + k_{29} \cdot H_2O_2 + k_{32} \cdot CO + k_{33} \cdot CH_4 + \\
219 \quad & k_{25} \cdot H_2 + k_{25} \cdot N) \quad (56)
\end{aligned}$$

220 Figure 2 shows height-latitude cross sections for the  $\langle OH/OH^{eq} \rangle$  ratio for each month. In this  
221 case, the equilibrium covers up to 70-80% of the presented ranges of heights and latitudes, so that the  
222 black solid lines mark the external bordersboundaries of non-equilibrium areas. In March and September,  
223 this area is almost symmetrical to the equator. In April-August, it is shifted towards the northern  
224 hemisphere. In October-February, this area is higher in the southern hemisphere. In all months, it is below  
225 85-86 km. In the polar regions, there are latitudinal ranges, where OH is close to equilibrium throughout  
226 the entire range of heights.

227

#### 228 **4 The main reactions, determining HO<sub>2</sub> and OH equilibriumsequilibria**

229 ~~The~~ Figure 3 showsresents height-latitude contour maps, showing the relative contribution of a  
230 certain reaction to the total source and sink of HO<sub>2</sub> in different monthsJanuary, taken foras an example.  
231 To increase the information content of the panels, the altitude range is cut off everywhere to 100 km10<sup>-3</sup>  
232 hPa, since there are no significant changes above. Note, first firstly, that reaction H+O<sub>2</sub>+M → HO<sub>2</sub>+M  
233 determines a major (up to 95% and more) contribution in the main equilibrium area almost everywhere,  
234 except for the polar regions above 70-75° of latitude and below 75-80 km, where the reactions OH+O<sub>3</sub> →  
235 O<sub>2</sub>+HO<sub>2</sub> and H<sub>2</sub>O<sub>2</sub>+OH → H<sub>2</sub>O+HO<sub>2</sub> become important and should be taken into account. ~~Second, other~~  
236 Other reactions (H<sub>2</sub>O<sub>2</sub>+O → OH+HO<sub>2</sub>, CHO+O<sub>2</sub> → HO<sub>2</sub>+CO, CH<sub>3</sub>O+O<sub>2</sub> → CH<sub>2</sub>O+HO<sub>2</sub>) together  
237 contribute less than 2-3% to the total source of HO<sub>2</sub> in the main equilibrium area and may be omitted.

238 ~~The Figure 4 presents height latitude contour maps showing the relative contribution of a certain~~  
239 ~~reaction to the total sink of HO<sub>2</sub> in the same months as in Figure 3. Firstly, it should be noted~~  
240 ~~that~~Secondly, the reaction HO<sub>2</sub>+O → OH+O<sub>2</sub> determines a major (up to 95% and more) contribution to  
241 the total sink in the main equilibrium area almost everywhere, except for the same small polar areas, as in  
242 the considered case with the sources, where the reactions HO<sub>2</sub>+O<sub>3</sub> → OH+2O<sub>2</sub> and NO+HO<sub>2</sub> → NO<sub>2</sub>+OH  
243 are important and should be taken into account. ~~Secondly, theThe~~ reactions OH+HO<sub>2</sub> → H<sub>2</sub>O+O<sub>2</sub>,  
244 H+HO<sub>2</sub> → 2OH, H+HO<sub>2</sub> → H<sub>2</sub>O+O, and H+HO<sub>2</sub> → H<sub>2</sub>+O<sub>2</sub> ~~give together~~ contribute cumulatively up to  
245 10-15% of the total sourcesink near the boundary of the main equilibrium area. ~~Thirdly, theThe~~ remaining  
246 reactions (HO<sub>2</sub>+HO<sub>2</sub> → H<sub>2</sub>O<sub>2</sub>+O<sub>2</sub>, HO<sub>2</sub>+HO<sub>2</sub>+M → H<sub>2</sub>O<sub>2</sub>+O<sub>2</sub>+M) are not important in the main  
247 equilibrium area and can be omitted.



Therefore, the expression for HO<sub>2</sub> local equilibrium concentration can be simplified as follows:

$$HO_2^{eq} = \frac{k_{20} \cdot H \cdot M \cdot O_2 + k_{22} \cdot OH \cdot O_3 + k_{29} \cdot H_2O_2 \cdot OH}{k_{18} \cdot O + k_{23} \cdot O_3 + k_{28} \cdot OH + (k_{14} + k_{15} + k_{16}) \cdot H + k_{50} \cdot NO} \quad (67)$$

~~Figures 5-6 show~~ Figure 4 presents height-latitude contour maps, showing the relative contribution of a certain reaction to the total source and sink of OH in ~~the same months as in Figure 3~~ January, taken ~~for as an~~ in Figure 3. As in the previous case, the altitude range is cut off at ~~100 km~~ 10<sup>-3</sup> hPa, because only the panels for the reactions H+O<sub>3</sub> → OH+O<sub>2</sub> and HO<sub>2</sub>+O → OH+O<sub>2</sub> consist of interesting variations ~~at the 100-130 km altitudes above~~. Note, that firstly these reactions are the main OH sources in the upper part of the presented distributions down to 70-75 km, where they jointly provide up to a 95% contribution ~~into the~~ equilibrium concentration. Also, the reaction HO<sub>2</sub>+O<sub>3</sub> → OH+2O<sub>2</sub> is major source in the lower part of the presented ~~distributions~~ distribution from 50 to 60-70 km, ~~depending on the month~~. The reaction NO+HO<sub>2</sub> → NO<sub>2</sub>+OH is important around non-equilibrium areas of OH and should be taken into account, whereas the reaction H +NO<sub>2</sub> → OH+NO is important in compact altitude-latitude areas near the poles, the reaction H+HO<sub>2</sub> → 2OH gives up to 10-15% contribution in small areas near the equilibrium boundary. Other reactions (O(<sup>1</sup>D)+H<sub>2</sub>O → 2OH, O(<sup>1</sup>D)+H<sub>2</sub> → H+OH, CH<sub>4</sub>+O(<sup>1</sup>D) → CH<sub>3</sub>+OH, H<sub>2</sub>O<sub>2</sub>+O → OH+HO<sub>2</sub>) together contribute less than 2-3% of the total source of OH in the main equilibrium area and can be omitted.

~~Figures 7-8 present height-latitude contour maps showing the relative contribution of a certain reaction to the total sink of OH. First, note that~~ Secondly, the reaction OH+O → H+O<sub>2</sub> is the main OH sink in the upper part of the presented distributions down to 70-80 km, ~~depending on the month~~, where it provides up to 95% of the equilibrium concentration. The reactions OH+CO → H+CO<sub>2</sub> and OH+O<sub>3</sub> → O<sub>2</sub>+HO<sub>2</sub> are major in the ~~lower~~ lower part of the presented distributions from 50 to 70-80 km, ~~depending on the month~~. The reaction OH+HO<sub>2</sub> → H<sub>2</sub>O+O<sub>2</sub> is ~~remarkable~~ significant enough around non-equilibrium areas of OH, whereas the reaction H<sub>2</sub>O<sub>2</sub>+OH → H<sub>2</sub>O+HO<sub>2</sub> is important in the compact altitude-latitude area near the poles. Other reactions (OH+OH → H<sub>2</sub>O+O, OH+H<sub>2</sub> → H<sub>2</sub>O+H, N+OH → NO+H, CH<sub>4</sub>+OH → CH<sub>3</sub>+H<sub>2</sub>O, H+OH+N<sub>2</sub> → H<sub>2</sub>O+N<sub>2</sub>, OH+OH+M → H<sub>2</sub>O<sub>2</sub>+M) together contribute less than 2-3% to the total ~~sources~~ sink of OH in the main equilibrium area and can be omitted.

Therefore, the expression for OH local equilibrium concentration can be ~~can be~~ simplified as follows:

$$OH^{eq} = \frac{k_{21} \cdot H \cdot O_3 + k_{18} \cdot O \cdot HO_2 + k_{23} \cdot HO_2 \cdot O_3 + 2 \cdot k_{14} \cdot H \cdot HO_2 + k_{24} \cdot H \cdot N_2 + k_{50} \cdot HO_2 \cdot NO + k_{51} \cdot NO_2 \cdot H}{k_{17} \cdot O + k_{22} \cdot O_3 + k_{28} \cdot HO_2 + k_{29} \cdot H_2O_2 + k_{32} \cdot CO} \quad (78)$$

## 5 Shortened equilibrium conditions of HO<sub>2</sub> and OH in the upper mesosphere and lower thermosphere

The above analysis revealed, that the reactions describing the equilibrium conditions (6-7-8) in the lower and middle mesosphere are ~~mainly~~ different from those in the upper mesosphere and lower thermosphere. This means that the task of applying these conditions can be divided into two parts depending on the selected altitude range. At the upper mesosphere and lower thermosphere altitudes, we can consider only the HO<sub>x</sub> – O<sub>x</sub> chemistry, excluding the reactions with participation of H<sub>2</sub>O<sub>2</sub>, N, NO, NO<sub>2</sub>, and CO. In addition, we can omit the reactions HO<sub>2</sub>+O<sub>3</sub> → OH+2O<sub>2</sub>, OH+O<sub>3</sub> → O<sub>2</sub>+HO<sub>2</sub>, and OH+HO<sub>2</sub> → H<sub>2</sub>O+O<sub>2</sub> due to their insignificance here. As ~~the~~ result, the shortened equilibrium conditions of HO<sub>2</sub> and OH for this altitude range are as follows:

$$HO_{2sh}^{eq} = \frac{k_{20} \cdot H \cdot M \cdot O_2}{k_{18} \cdot O + (k_{14} + k_{15} + k_{16}) \cdot H} \quad (89)$$

$$OH_{sh}^{eq} = \frac{k_{21} \cdot H \cdot O_3 + k_{18} \cdot O \cdot HO_2 + 2 \cdot k_{14} \cdot H \cdot HO_2}{k_{17} \cdot O} \quad (910)$$

~~The~~ Figure 95 shows height-latitude cross sections for the  $\langle HO_2/HO_{2sh}^{eq} \rangle$  ratio for each month. In each panel, the upper longest black line marks the lower ~~border~~boundary of the main equilibrium area, where, according to condition (1);  $HO_2 \approx HO_{2sh}^{eq}$  with possible bias of less than 10%. As in the case of Figure 1, this area extends from the top of the analyzed altitude range. There are also very small equilibrium areas below, which can be omitted from our consideration. The height of the lower ~~border~~boundary of the main equilibrium area,  $z_{HO_{2sh}^{eq}}^{eq}$ , depends essentially on the season and latitude. Comparing with Figure 1, one can see, ~~that it repeats well~~reproduces many features of  $z_{HO_{2sh}^{eq}}$  at low and middle latitudes. In particular,  $z_{HO_{2sh}^{eq}}$  varies in the interval between 73 and 85 km, as in the case of  $z_{HO_2^{eq}}$ . In the middle latitudes,  $z_{HO_{2sh}^{eq}}$  in summer is several km higher than in winter. Near ~~the~~ equator,  $z_{HO_{2sh}^{eq}}$  demonstrates the weakest annual variations and varies in the range of 81-83 km. So, one can conclude, that the exclusion of a number of reactions does not lead to significant changes in the space-time distributions of the HO<sub>2</sub> equilibrium.

~~The~~ Figure 106 plots height-latitude cross sections for the  $\langle OH/OH_{sh}^{eq} \rangle$  ratio for each month. As in the previous case, this is the lower ~~border~~boundary of the equilibrium area, where, according to condition (1);  $OH \approx OH_{sh}^{eq}$  with good precision. The dependence of the ~~border~~boundary height,  $z_{OH_{sh}^{eq}}$ , on the season and latitude mainly repeats ~~mainly the behavior of~~  $z_{HO_{2sh}^{eq}}$ . In particular,  $z_{OH_{sh}^{eq}}$  varies in the interval between 73 and 85 km. At middle latitudes,  $z_{OH_{sh}^{eq}}$  in summer is several km higher than in winter. Near the equator,  $z_{OH_{sh}^{eq}}$  also demonstrates the weakest annual variations and varies in the range of 81-83

km. Nevertheless, in some cases, the OH equilibrium ~~borderboundary~~ lies slightly higher than the HO<sub>2</sub> ~~borderboundary~~. In particular, it can be seen in April-August above 50°S, which can be explained by the difference between HO<sub>2</sub> and OH lifetimes ( $\tau_{HO_2} < \tau_{OH}$ ), mainly, due to  $k_{18} > k_{17}$ . Comparing with Figure 2, one can see ~~that~~ the exclusion of the mentioned reactions from consideration results in the absence of the OH equilibrium areas at the low and middle mesosphere altitudes, as expected.

## 6 The ~~criteria~~ criteria for HO<sub>2</sub> and OH equilibrium validity in the upper mesosphere and lower thermosphere

~~Let~~ Firstly we determine HO<sub>2</sub> and OH lifetimes and the local time scales of  $HO_{2sh}^{eq}$  and  $OH_{sh}^{eq}$ , according to Section 2.

From ~~(8Eqs. (2-3) and (9))~~, HO<sub>2</sub> lifetime and the local time scales of  $HO_{2sh}^{eq}$  are as follows:

$$\tau_{HO_2} = \frac{1}{k_{18} \cdot O + (k_{14} + k_{15} + k_{16}) \cdot H} \quad (10)$$

$$\tau_{HO_2}^{eq} = \frac{1}{k_{18} \cdot O + (k_{14} + k_{15} + k_{16}) \cdot H} \quad (11)$$

$$\tau_{HO_2sh}^{eq} = \frac{HO_{2sh}^{eq}}{|dHO_{2sh}^{eq}/dt|} \quad (12)$$

~~Let~~ Then we find the expression for  $dHO_{2sh}^{eq}/dt$ :

$$\frac{dHO_{2sh}^{eq}}{dt} = \frac{k_{18} \cdot k_{20} \cdot M \cdot O_2 \cdot \frac{d}{dt} \left( \frac{H}{O} \right) \cdot O^2}{(k_{18} \cdot O + (k_{14} + k_{15} + k_{16}) \cdot H)^2} = - \frac{k_{18} \cdot k_{20} \cdot M \cdot O_2 \cdot \frac{d}{dt} \left( \frac{O}{H} \right) \cdot H^2}{(k_{18} \cdot O + (k_{14} + k_{15} + k_{16}) \cdot H)^2} \quad (12)$$

$$\frac{k_{18} \cdot k_{20} \cdot M \cdot O_2 \cdot \frac{d}{dt} \left( \frac{O}{H} \right) \cdot H^2}{(k_{18} \cdot O + (k_{14} + k_{15} + k_{16}) \cdot H)^2} \quad (13)$$

Kulikov et al. (2023a) analyzed ~~analytically~~ the local nighttime evolution of O and H within the framework of pure HO<sub>x</sub> – O<sub>x</sub> chemistry and found the expression for  $\frac{d}{dt} \left( \frac{O}{H} \right)$ :

$$\frac{d}{dt} \left( \frac{O}{H} \right) = -2 \cdot k_{20} \cdot M \cdot O_2 \cdot \left( 1 - \frac{k_{15} + k_{16}}{k_{18}} \right) - k_{21} \cdot O_3 - k_{12} \cdot M \cdot O_2 \cdot \frac{O}{H} \quad (1314)$$

Thus, ~~the expression (12Eq. (13))~~ can be rewritten in the following form:

$$\frac{dHO_{2sh}^{eq}}{dt} = \frac{k_{18} \cdot k_{20} \cdot M \cdot O_2 \cdot H^2 \cdot \left(2 \cdot k_{20} \cdot M \cdot O_2 \cdot \left(1 - \frac{k_{15} + k_{16}}{k_{18}}\right) + k_{21} \cdot O_3 + k_{12} \cdot M \cdot O_2 \cdot \frac{O}{H}\right)}{(k_{18} \cdot O + (k_{14} + k_{15} + k_{16}) \cdot H)^2}$$

(14)

$$\frac{k_{18} \cdot k_{20} \cdot M \cdot O_2 \cdot H^2 \cdot \left(2 \cdot k_{20} \cdot M \cdot O_2 \cdot \left(1 - \frac{k_{15} + k_{16}}{k_{18}}\right) + k_{21} \cdot O_3 + k_{12} \cdot M \cdot O_2 \cdot \frac{O}{H}\right)}{(k_{18} \cdot O + (k_{14} + k_{15} + k_{16}) \cdot H)^2}$$

(15)

By combining (8), (14), (9), (12), and (15) we obtain the expression for the local time scales of

$HO_{2sh}^{eq}$ :

$$\tau_{HO_{2sh}^{eq}} \tau_{HO_{2sh}^{eq}} = \frac{(k_{18} \cdot O + (k_{14} + k_{15} + k_{16}) \cdot H)}{k_{18} \cdot H \cdot \left(2 \cdot k_{20} \cdot M \cdot O_2 \cdot \left(1 - \frac{k_{15} + k_{16}}{k_{18}}\right) + k_{21} \cdot O_3 + k_{12} \cdot M \cdot O_2 \cdot \frac{O}{H}\right)} \cdot \frac{(k_{18} \cdot O + (k_{14} + k_{15} + k_{16}) \cdot H)}{k_{18} \cdot H \cdot \left(2 \cdot k_{20} \cdot M \cdot O_2 \cdot \left(1 - \frac{k_{15} + k_{16}}{k_{18}}\right) + k_{21} \cdot O_3 + k_{12} \cdot M \cdot O_2 \cdot \frac{O}{H}\right)}$$

(1516)

Thus, taking into account (3), (10), (4), (11) and (1516), the criterion for  $HO_2$  equilibrium validity is written in the form:

$$Crit_{HO_2} = \frac{\tau_{HO_2}}{\tau_{HO_{2sh}^{eq}}} = \frac{k_{18} \cdot H \cdot \left(2 \cdot k_{20} \cdot M \cdot O_2 \cdot \left(1 - \frac{k_{15} + k_{16}}{k_{18}}\right) + k_{21} \cdot O_3 + k_{12} \cdot M \cdot O_2 \cdot \frac{O}{H}\right)}{(k_{18} \cdot O + (k_{14} + k_{15} + k_{16}) \cdot H)^2} \leq 0.1$$

(16)

$$\frac{k_{18} \cdot H \cdot \left(2 \cdot k_{20} \cdot M \cdot O_2 \cdot \left(1 - \frac{k_{15} + k_{16}}{k_{18}}\right) + k_{21} \cdot O_3 + k_{12} \cdot M \cdot O_2 \cdot \frac{O}{H}\right)}{(k_{18} \cdot O + (k_{14} + k_{15} + k_{16}) \cdot H)^2} \leq 0.1$$

(17)

We calculated  $Crit_{HO_2}$  using the global 3D chemical transport model<sub>2</sub> and included the zonally and monthly averaged lines  $\langle Crit_{HO_2} \rangle \geq 0.1$  in Figure 95 (see magenta lines). One can see that, depending on the month, each ~~red~~magenta line ~~well~~ reproduces well the lower ~~border~~boundary of the main ~~OH~~HO<sub>2</sub> equilibrium area and ~~repeats~~follows almost all its features and variations. Note<sub>2</sub> that, in ~~zero~~the zeroth order approximation, the criterion (1617) can be simplified as

$$Crit_{HO_2} \approx \left(2 \cdot k_{20} \cdot M \cdot O_2 \cdot \left(1 - \frac{k_{15} + k_{16}}{k_{18}}\right) + k_{21} \cdot O_3 + k_{12} \cdot M \cdot O_2 \cdot \frac{O}{H}\right) \cdot \frac{H}{k_{18} \cdot O^2} \leq 0.1$$

(1718)

From (9), (2-3) and (10), OH lifetime and the local time scales of  $OH_{sh}^{eq}$  are as follows:

$$\tau_{OH} = \frac{1}{k_{17} \cdot O} \cdot \frac{1}{k_{17} \cdot O}$$

(1819)

$$\tau_{OH_{sh}^{eq}} = \frac{OH_{sh}^{eq}}{|dOH_{sh}^{eq}/dt|}. \quad (1920)$$

)  
 Before determining the expression for  $dOH_{sh}^{eq}/dt$ , ~~first of all~~, one should ~~to~~ keep in mind, that the expression (910) depends on the  $HO_2$  concentration. ~~Above~~As previously mentioned, ~~that~~ near and above the OH equilibrium ~~border, boundary~~  $HO_2$  is in equilibrium ( $HO_2 \approx HO_{2sh}^{eq}$ ) and we can use ~~expression~~ (8Eq. (9)). In view of  $k_{18} \cdot O \gg (k_{14} + k_{15} + k_{16}) \cdot H$ ,

$$HO_{2sh}^{eq} \approx \frac{k_{20} \cdot H \cdot M \cdot O_2}{k_{18} \cdot O} \left(1 - \frac{(k_{14} + k_{15} + k_{16}) \cdot H}{k_{18} \cdot O}\right). \quad (2021)$$

)  
 The substitution of (20Eq. (21)) into (9Eq. (10)) yields:

$$OH_{sh}^{eq} = k_{20} \cdot H \cdot M \cdot O_2 \cdot \frac{(1 + \frac{2 \cdot k_{14} \cdot H}{k_{18} \cdot O}) \cdot (1 - \frac{(k_{14} + k_{15} + k_{16}) \cdot H}{k_{18} \cdot O})}{k_{17} \cdot O} + \frac{k_{21} \cdot H \cdot O_3}{k_{17} \cdot O} \approx \frac{k_{20} \cdot H \cdot M \cdot O_2}{k_{17} \cdot O} \cdot \left(1 + \frac{(k_{14} - k_{15} - k_{16}) \cdot H}{k_{18} \cdot O} \cdot \frac{(k_{14} - k_{15} - k_{16}) \cdot H}{k_{18} \cdot O}\right) + \frac{k_{21} \cdot H \cdot O_3}{k_{17} \cdot O} \quad (2122)$$

)  
 Thus, the expression for  $dOH_{sh}^{eq}/dt$  is:

$$\frac{dOH_{sh}^{eq}}{dt} = \frac{d}{dt} \left(\frac{H}{O}\right) \cdot \left(\frac{k_{20} \cdot M \cdot O_2}{k_{17}} \cdot \left(1 + \frac{2 \cdot (k_{14} - k_{15} - k_{16}) \cdot H}{k_{18} \cdot O}\right) + \frac{k_{21} \cdot O_3}{k_{17}}\right) + \frac{k_{21} \cdot H}{k_{17} \cdot O} \frac{dO_3}{dt}. \quad (2223)$$

)  
 Taking into account (13Eq. (14)) and the differential equation for  $O_3$  time evolution:

$$\frac{dO_3}{dt} = k_{12} \cdot M \cdot O_2 \cdot O - k_{21} \cdot H \cdot O_3,$$

the expression (2123) can be rewritten in following form:

$$\frac{dOH_{sh}^{eq}}{dt} = \frac{(2 \cdot k_{20} \cdot M \cdot O_2 \cdot \left(1 - \frac{k_{15} + k_{16}}{k_{18}}\right) + k_{21} \cdot O_3 + k_{12} \cdot M \cdot O_2 \cdot \frac{O}{H}) \cdot \frac{H^2}{O^2} \left(\frac{k_{20} \cdot M \cdot O_2}{k_{17}} \cdot \left(1 + \frac{2 \cdot (k_{14} - k_{15} - k_{16}) \cdot H}{k_{18} \cdot O}\right) + \frac{k_{21} \cdot O_3}{k_{17}}\right) + \frac{k_{21} \cdot H \cdot (k_{12} \cdot M \cdot O_2 \cdot O - k_{21} \cdot H \cdot O_3)}{k_{17} \cdot O}}{O^2} \cdot \left(\frac{k_{20} \cdot M \cdot O_2}{k_{17}} \cdot \left(1 + \frac{2 \cdot (k_{14} - k_{15} - k_{16}) \cdot H}{k_{18} \cdot O}\right) + \frac{k_{21} \cdot O_3}{k_{17}}\right) + \frac{k_{21} \cdot H \cdot (k_{12} \cdot M \cdot O_2 \cdot O - k_{21} \cdot H \cdot O_3)}{k_{17} \cdot O}.$$

(2324)

Thus, by combining (3), (18Eqs. (4), (19), (2420), (22), and (2324) we obtain the expression for the criterion for OH equilibrium validity:

$$\begin{aligned}
 Crit_{OH} &= \frac{\tau_{OH}}{\tau_{OH_{sh}^{eq}}} = \frac{1}{k_{17} \cdot O} \cdot \left( \left( 2 \cdot k_{20} \cdot M \cdot O_2 \cdot \left( 1 - \frac{k_{15} + k_{16}}{k_{18}} \right) + k_{21} \cdot O_3 + k_{12} \cdot M \cdot O_2 \cdot \frac{O}{H} \right) \cdot \frac{H}{O} \right. \\
 &\quad \left. \left( k_{20} \cdot M \cdot O_2 \cdot \left( 1 + \frac{2 \cdot (k_{14} - k_{15} - k_{16}) \cdot H}{k_{18} \cdot O} \right) + k_{21} \cdot O_3 \right) + k_{21} \cdot (k_{12} \cdot M \cdot O_2 \cdot O - k_{21} \cdot H \cdot O_3) \right) / (k_{20} \cdot M \cdot \\
 &\quad O_2 \cdot \left( 1 + \frac{(k_{14} - k_{15} - k_{16}) \cdot H}{k_{18} \cdot O} \right) + k_{21} \cdot O_3) \leq 0.1.
 \end{aligned}
 \tag{24}$$

$$\begin{aligned}
 &\frac{\left( \left( 2 \cdot k_{20} \cdot M \cdot O_2 \cdot \left( 1 - \frac{k_{15} + k_{16}}{k_{18}} \right) + k_{21} \cdot O_3 \cdot \frac{H}{O} + k_{12} \cdot M \cdot O_2 \right) \cdot \left( k_{20} \cdot M \cdot O_2 \cdot \left( 1 + \frac{2 \cdot (k_{14} - k_{15} - k_{16}) \cdot H}{k_{18} \cdot O} \right) + k_{21} \cdot O_3 \right) + k_{21} \cdot (k_{12} \cdot M \cdot O_2 \cdot O - k_{21} \cdot H \cdot O_3) \right)}{k_{17} \cdot O \cdot \left( k_{20} \cdot M \cdot O_2 \cdot \left( 1 + \frac{(k_{14} - k_{15} - k_{16}) \cdot H}{k_{18} \cdot O} \right) + k_{21} \cdot O_3 \right)} \leq \\
 &0.1.
 \end{aligned}
 \tag{25}$$

We calculated  $Crit_{OH}$ , using the global 3D chemical transport model<sub>1</sub> and included the zonally and monthly averaged lines  $\langle Crit_{OH} \rangle = 0.1$  in Figure 106 (see magenta lines). One can see that, depending on the month, ~~red~~ the magenta line almost everywhere reproduces the lower ~~border~~ boundary of the OH equilibrium area and repeats mainly its features and variations. Nevertheless, there are a few (by latitude) narrow areas (in April-August near 70°S and in October-December near 70°N)<sub>2</sub>, where the criterion gives a few km lower position of the OH equilibrium boundary, ~~that is going to be~~ these are discussed ~~below in~~ the next section. Note, ~~that~~ our numerical analysis shows that, in ~~zero~~ the zeroth order approximation, the criterion (2425) can be simplified as:

$$\begin{aligned}
 Crit_{OH} &\approx \left( 2 \cdot k_{20} \cdot M \cdot O_2 \cdot \left( 1 - \frac{k_{15} + k_{16}}{k_{18}} \right) + k_{21} \cdot O_3 + k_{12} \cdot M \cdot O_2 \cdot \frac{O}{H} \right) \left( 2 \cdot k_{20} \cdot M \cdot O_2 \cdot \left( 1 - \right. \right. \\
 &\quad \left. \left. \frac{k_{15} + k_{16}}{k_{18}} \right) + k_{21} \cdot O_3 + k_{12} \cdot M \cdot O_2 \cdot \frac{O}{H} \right) \cdot \frac{H}{k_{17} \cdot O^2} \leq 0.1.
 \end{aligned}
 \tag{2526}$$

## 7 Discussion

Let's We now discuss obtained results and their possible applications.

Pay attention to the fact, that the presented results were plotted, using the lower threshold at 105° for the nighttime solar zenith angle ( $\chi$ ) to exclude the twilight transition processes. Nevertheless, our additional analysis revealed, that OH and HO<sub>2</sub> equilibrium conditions are fulfilled at  $\chi > 95^\circ$ . Evidently, during the

processing of the measurement data, taking twilight  $\chi$  in (95°,105°) range into account extends the latitude range of OH and HO<sub>2</sub> equilibria application and allows us to include a noticeable part of the data into consideration. However, in this case one should check for additional condition (Kulikov et al., 2023a):

$$e^{\int_{lt_{bn}}^{lt} \tau_{HO_2}^{-1} dt} \gg 1, e^{\int_{lt_{bn}}^{lt} \tau_{OH}^{-1} dt} \gg 1, \quad (27)$$

where  $\tau_{HO_2}$  and  $\tau_{OH}$  are the HO<sub>2</sub> and OH lifetimes, determined by Eqs. (11) and (19),  $lt$  is local time of data,  $lt_{bn}$  is the local time at the beginning of the night. Mind, that at night O and H tend to decrease due to the shutdown of the O<sub>x</sub> and HO<sub>x</sub> family photochemical sources, so  $\tau_{HO_2}$  and  $\tau_{OH}$  increase. Thus, analyzing the measurement data one can apply more stringent conditions:

$$e^{\frac{lt-lt_{bn}}{\tau_{HO_2}}} \gg 1, e^{\frac{lt-lt_{bn}}{\tau_{OH}}} \gg 1, \quad (28)$$

The main results were obtained using a 3D model, where temperature and wind distributions are updated every 24 hours. This excluded the influence of the atmospheric wave motion, in particular, associated with tides, which is one of the main dynamical drivers in the tropical mesopause. We carried out additional modeling with the distributions of the main characteristics, calculated by the Canadian Middle Atmosphere Model for the year 2009 (Scinocca et al., 2008) with a 6-hourly frequency for updating. The analysis of the time-height evolution of OH and HO<sub>2</sub>, especially at low latitudes, showed that our criteria reproduce quite well the local variations of the OH and HO<sub>2</sub> equilibrium boundaries in such conditions.

We evaluated the sensitivity of the presented HO<sub>2</sub> and OH criteria ( $Crit_{HO_2}$  and  $Crit_{OH}$ ) to the uncertainties of characteristics, involved in the expressions (17) and (25). The local heights of the OH and HO<sub>2</sub> equilibrium boundaries ( $z_{HO_2}^{crit}$  and  $z_{OH}^{crit}$ ) according to the criteria are determined as the altitudes, at which  $Crit_{HO_2} = 0.1$  and  $Crit_{OH} = 0.1$  respectively. We considered the whole dataset of nighttime profiles, obtained by the numerical simulation of a one-year global evolution of mesosphere – lower thermosphere, and estimated total uncertainties to determination of  $z_{HO_2}^{crit}$  and  $z_{OH}^{crit}$  from each local (in time and space) dataset (profiles of O, H, O<sub>3</sub>, M, O<sub>2</sub> and temperature). Following the typical analysis presented, for example in Mlynczak et al. (2013a, 2014), each uncertainty was calculated as a root sum square of the sensitivities to the individual perturbations of certain variables or parameters in the expressions (17) and (25). The following uncertainties of the variables were used: 5K in the temperature and 30% in O<sub>3</sub>, O, and H. The uncertainties in reaction rates and their temperature dependencies were taken from Burkholder et al. (2020). As the result (see Figure 7), the monthly and longitudinally mean of total uncertainties in determination of  $z_{HO_2}^{crit}$  and  $z_{OH}^{crit}$  were found varying in the range 0.02-1 km, depending on altitude and season. Note, that these values are comparable with the typical height

447 resolution of satellite data. The latter allows us to consider our criteria as a robust instrument for  
 448 equilibrium condition validation. The main reason of relatively low sensitivity of  $z_{HO_2}^{crit}$  and  $z_{OH}^{crit}$  is  
 449 the strong height-dependence of  $Crit_{HO_2}$  and  $Crit_{OH}$  near the value of 0.1.

450 As noted, ~~Figures 9-10 present~~ Figs. 5-6 represent an interesting peculiarity. At the middle latitudes,  
 451 summer  $z_{HO_2}^{eq}$  and  $z_{OH}^{eq}$  are ~~several km~~ remarkably higher than winter ones. Recently ~~(Kulikov et al.,~~  
 452 (2023b) found such a feature ~~was found~~ in the evolution of nighttime ozone chemical equilibrium  
 453 boundary, derived from SABER/TIMED data, ~~which was which was~~ accompanied by the same variation of  
 454 the transition zone ~~dividing, separating~~ deep and weak photochemical oscillations of O and H, caused by  
 455 the diurnal variations of solar radiation. ~~Kulikov et al. (2023b) The authors~~ analyzed this effect  
 456 ~~analytically and~~ near and below the transition zone. It was shown firstly, that nighttime O decreases with  
 457 the characteristic time scale  $\tau_O = O/|dO/dt|$  proportional to the  $O/H$  ratio at the beginning of the night.  
 458 Secondly, during the summer the daytime  $O/H$  at the middle latitudes is remarkably less than the one in  
 459 winter. Consequently, summer values of  $\tau_O$  are significantly shorter than winter ones, so summer O  
 460 during the night decreases much faster than in winter. In our case lifetimes of  $HO_2$  and OH are  
 461 proportional mainly to  $\frac{1}{O}$  (see Eqs. (11) and (19)), so the summer rise of  $z_{HO_2}^{eq}$  and  $z_{OH}^{eq}$  can be  
 462 explained by the markedly lower values of the O and H nighttime evolution times in summer than in  
 463 winter by virtue, mainly, of the lower values of the  $O/H$  ratio during the night, which, in turn, is  
 464 determined by the daytime photochemistry. At middle, the ozone boundary varies within 4-5 km interval  
 465 above 80 km, whereas the range of OH and  $HO_2$  boundaries variations is 72-85 km (see Figures 9-10). In  
 466 the case of ozone, its criterion for equilibrium validity (see (5) in Kulikov et al. (2023b)) is as  
 467 follows: season difference in O diurnal evolution at these latitudes.

$$468 \quad Crit_{O_3} = 2 \frac{k_{12} \cdot O_2 \cdot M}{k_{21}} \left( k_{20} \cdot M \cdot O_2 \cdot \left( 1 - \frac{k_{15} + k_{16}}{k_{18}} \right) + k_{21} \cdot O_3 \right) \cdot \frac{1}{k_{21} \cdot H \cdot O_3} \leq 0.1. \quad (26)$$

469 At  $O_3 \approx O_3^{eq} = \frac{k_{12} \cdot M \cdot O_2 \cdot O}{k_{21} \cdot H}$ , one can see that  $Crit_{O_3} \sim \frac{1}{O}$ . It is follows from simplified expressions (17) and  
 470 (25) that  $Crit_{HO_2}$  and  $Crit_{OH}$  are proportional to  $\frac{H}{O^2}$ . Such dependence leads to a stronger annual variation  
 471 of OH and  $HO_2$  equilibrium boundaries than in the case of  $O_3$ .

472 As noted, there are a few narrow areas near  $70^\circ S/N$  (Figure ~~10~~ 6), where the criterion (25) does not  
 473 agree ~~correspond~~ well with ~~to~~ the OH equilibrium boundary. Our analysis revealed, that the main reason is  
 474 neglecting the reaction  $OH + CO \rightarrow H + CO_2$  as the source of H in the corresponding differential equation  
 475 of its chemical balance. In order to improve the criterion, we revised the derivation of expression ~~(17)~~ (14)  
 476 for  $\frac{d}{dt} \left( \frac{O}{H} \right)$  following to Kulikov et al. (2023a):



$$\frac{d}{dt} \left( \frac{O}{H} \right) = -2 \cdot k_{20} \cdot M \cdot O_2 \cdot \left( 1 - \frac{k_{15} + k_{16}}{k_{18}} \right) - k_{21} \cdot O_3 - k_{12} \cdot M \cdot O_2 \cdot \frac{O}{H} - \frac{k_{32} \cdot CO}{k_{17} \cdot H} \cdot (k_{20} \cdot M \cdot O_2 \cdot (1 + \frac{(k_{14} - k_{15} - k_{16}) \cdot H}{k_{18} \cdot O}) + k_{21} \cdot O_3)).$$

(2729)

As thea result, the corrected criterion for OH equilibrium validity is as follows:

$$Crit_{OH}^m = \frac{1}{k_{17} \cdot O} \cdot \left( 2 \cdot k_{20} \cdot M \cdot O_2 \cdot \left( 1 - \frac{k_{15} + k_{16}}{k_{18}} \right) + k_{21} \cdot O_3 + k_{12} \cdot M \cdot O_2 \cdot \frac{O}{H} + \frac{k_{32} \cdot CO}{k_{17} \cdot H} \cdot (k_{20} \cdot M \cdot O_2 \cdot (1 + \frac{(k_{14} - k_{15} - k_{16}) \cdot H}{k_{18} \cdot O}) + k_{21} \cdot O_3) \right) \leq 0.1. \quad (28)$$

$$Crit_{OH}^m = \frac{2 \cdot k_{20} \cdot M \cdot O_2 \cdot \left( 1 - \frac{k_{15} + k_{16}}{k_{18}} \right) + k_{21} \cdot O_3 + k_{12} \cdot M \cdot O_2 \cdot \frac{O}{H} + \frac{k_{32} \cdot CO}{k_{17} \cdot H} \cdot (k_{20} \cdot M \cdot O_2 \cdot (1 + \frac{(k_{14} - k_{15} - k_{16}) \cdot H}{k_{18} \cdot O}) + k_{21} \cdot O_3)}{k_{17} \cdot O \cdot (k_{20} \cdot M \cdot O_2 \cdot (1 + \frac{(k_{14} - k_{15} - k_{16}) \cdot H}{k_{18} \cdot O}) + k_{21} \cdot O_3)} \cdot \frac{H}{O} \cdot \left( k_{20} \cdot M \cdot O_2 \cdot \left( 1 + \frac{2 \cdot (k_{14} - k_{15} - k_{16}) \cdot H}{k_{18} \cdot O} \right) + k_{21} \cdot O_3 \right) + \frac{k_{21} \cdot (k_{12} \cdot M \cdot O_2 \cdot O - k_{21} \cdot H \cdot O_3)}{k_{17} \cdot O \cdot (k_{20} \cdot M \cdot O_2 \cdot (1 + \frac{(k_{14} - k_{15} - k_{16}) \cdot H}{k_{18} \cdot O}) + k_{21} \cdot O_3)} \leq 0.1 \quad (30)$$

We calculated this criterion, using the global 3D chemical transport model and included the zonally and monthly averaged lines  $\langle Crit_{OH}^m \rangle = 0.1$  on the OH equilibrium maps (see Figure 448). One can see that including, the inclusion of this additional term actually eliminates the noted discrepancy between OH boundary and criterion. But, the application of this criterion requires CO data.

As noted in the Introduction, the conditions of nighttime OH and HO<sub>2</sub> equilibriumsequilibria together with one for O<sub>3</sub> equilibrium and their analytical criteria constitute thea useful tool for to retrieval of these components or other characteristics (for example, O and H) from measured data. At the altitudes of upper mesosphere – lower thermosphere, these conditions can be applied, for example, to MLS/Aura database (measured characteristics: OH, HO<sub>2</sub>, O<sub>3</sub>, and CO), SMILES (HO<sub>2</sub> and O<sub>3</sub>), SCIAMACHY (O(<sup>1</sup>S) green-line, O<sub>2</sub> A-band, and OH Meinel band emissions), SABER/TIMED (O<sub>3</sub>, OH Meinel band emissions at 2.0 μm (9→7 and 8→6 bands) and at 1.6 μm (5→3 and 4→2 bands)) and other, including to improveimprovement of existing retrieval approaches. In particular, Panka et al. (2021) proposed the method of simultaneous derivation of O and OH at the levels v=0-9 from SABER data (volume emission rates at 2.0 and 1.6 μm), VER<sub>2μm</sub> and VER<sub>1.6μm</sub> at 80-100 km, taking into account the equilibrium condition for all states of OH. Such approach is valid for exitedexcited states due to itstheir very lowshort lifetimes determined by radiative transitions and quenching with O<sub>2</sub>, N<sub>2</sub>, and O. In the case of the OH ground state, its lifetimeslifetime is determined by the reaction OH+O → H+O<sub>2</sub> only. It means, that

Panka et al. (2021) used an equilibrium condition for total OH, which, as one can see from Figure 6, may be significantly disrupted above 80 km in certain. On the other hand, there are latitude ranges and seasons, as one can see from Figure 8. In order to check this assumption, we processed months, when the OH equilibrium boundary drops remarkably below 80 km. Moreover, the Panka et al. (2021) method requires external data (about HO<sub>2</sub>, since the reaction HO<sub>2</sub>+O → OH(v=9), +O<sub>2</sub>, N<sub>2</sub>, and temperature profiles at 80–100 km) becomes the important source for 2009 and calculated local profiles of Crit<sub>OH</sub> according to criterion (24). One can see this criterion depends of O, H, and O<sub>3</sub>. Thus, the O<sub>3</sub> data was taken from SABER data collocated (via the orbit number) with the OH below 87 km (Panka et al. profiles in time and space. The H data was derived with the use of the equilibrium equation for OH(v=9);, 2021; see also Figure 4 in our paper).

$$a_7 \cdot O_3 \cdot H = OH(9) \cdot (a_1 + a_2 \cdot N_2 + a_3 \cdot O_2 + (a_4 + a_5 + a_6) \cdot O), \quad (29)$$

The results of our paper allow modifying the Panka et al. method to extend its capabilities. The simplest development of this method seems to be the following. First of all, note that the HO<sub>2</sub> equilibrium condition (9) depends on H and O only and can be used within the self-consistent retrieval procedure, considering the following system of equations:

$$OH(v = 1 - 9) = \frac{k_{12} \cdot H \cdot O_3 \cdot M \cdot f(v) + \sum_{v' > v} (a_1(v', v) + a_2(v', v) \cdot O_2 + a_3(v', v) \cdot N_2 + (a_4(v', v) + a_5(v', v)) \cdot O) \cdot OH(v')}{a_6(v) \cdot O + \sum_{v' > v} (a_1(v, v') + a_2(v, v') \cdot O_2 + a_3(v, v') \cdot N_2 + (a_4(v, v') + a_5(v, v')) \cdot O)} \quad 2$$

$$OH(0) = \frac{\sum_{v' > 0} (a_1(v', 0) + a_2(v', 0) \cdot O_2 + a_3(v', 0) \cdot N_2 + (a_4(v', 0) + a_5(v', 0)) \cdot O) \cdot OH(v') + k_{18} \cdot O \cdot HO_2 + 2 \cdot k_{14} \cdot H \cdot HO_2}{k_{17} \cdot O} \quad 2$$

$$HO_2 = \frac{k_{20} \cdot H \cdot M \cdot O_2}{k_{18} \cdot O + (k_{14} + k_{15} + k_{16}) \cdot H^2}$$

$$VER_{2\mu m} = a_1(9, 7) \cdot OH(9) + a_1(8, 9) \cdot OH(8),$$

$$VER_{1.6\mu m} = a_1(5, 3) \cdot OH(5) + a_1(4, 2) \cdot OH(4),$$

where  $a_{1-6}$  are the constant rates of the processes OH(9v) → OH(v' < v ≤ 8) + hv, OH(9v) + O<sub>2</sub> → OH(v < v') + O<sub>2</sub>, OH(v) + N<sub>2</sub> → OH(8v < v') + N<sub>2</sub>, OH(9) + O<sub>2</sub> → OH(v ≤ 8) + O<sub>2</sub>, OH(9v) + O(<sup>3</sup>P) → OH(v' < v ≤ 4-5) + O(<sup>1</sup>D), OH(9v) + O(<sup>3</sup>P) → OH(v' < v ≤ 8) + O(<sup>3</sup>P), and OH(v) + O(<sup>3</sup>P) → H + O<sub>2</sub>, and H + O<sub>3</sub> → O<sub>2</sub> + OH(9), respectively. The values of  $a_{2-7}$  correspond to the Panka et al. (2021) model (see Table 1 there), the Einstein coefficients for OH(v=9) were taken from Brooke et al. (2016). Due to the strong air concentration dependence Crit<sub>OH</sub> decreases rapidly. Take into consideration, that this system includes 13 equations with the height. From each Crit<sub>OH</sub> profile 13 unknown variables. Therefore, the solution to the system for a single set of the SABER measurements (simultaneously measured profiles of O<sub>3</sub>, T, pressure, VER<sub>2μm</sub>, and VER<sub>1.6μm</sub>) gives one simultaneously retrieved profiles of O, H, OH(v=0-9), and HO<sub>2</sub>. By applying the criteria (17) and (25) to obtained O and H profiles, we determined the local height position of the OH equilibrium boundary ( $z_{OH_{sh}^{eq}}$ ) according to the condition Crit<sub>OH</sub> = 0.1. It was revealed that Crit<sub>OH</sub> < 0.1 throughout the entire altitude range for most profiles. The Figure 12 plots the

536 found values of  $z_{OH}^{eq}$  above 80 km in different months. One can see that, in accordance of the Panka et  
537 al. data, verify the local height position of the OH equilibrium boundary can rise up to 87 km. Moreover,  
538 the Panka et al. method requires external data about HO<sub>2</sub> since the reaction HO<sub>2</sub>+O → OH+O<sub>2</sub> become  
539 the important source for OH below 87 km (Panka et al., 2021; see also Figure 5 in our paper). Note that  
540 the fulfillment of OH and HO<sub>2</sub> equilibrium condition (8) depends on H conditions and O only and can be  
541 used within determine the general height, below which the resulting profiles should be cut. More advanced  
542 retrieval procedure of O, H, OH( $v=0-9$ ), and HO<sub>2</sub> would be statistical, based on Bayesian theorem, taking  
543 into account the criteria (16) and (24). uncertainties in measurement data and rate constants. Similarly, for  
544 example, to Kulikov et al. (2018a), it should include a derivation of posterior conditional probability  
545 density function of retrieved characteristics and numerical analysis of this function. Detailed development  
546 of this retrieval method is outside of this paper and should be carried out in a separate extended work.

## 549 8 Conclusions

550 The presented analysis shows, that there are extended areas in mesosphere and lower thermosphere,  
551 where nighttime HO<sub>2</sub> and OH are close to their local equilibrium concentrations, determined mainly by  
552 the reaction reactions between HO<sub>x</sub> – O<sub>x</sub> components among themselves and with H<sub>2</sub>O<sub>2</sub>, N, NO, NO<sub>2</sub>, and  
553 CO. In upper mesosphere – lower thermosphere, the shortened expressions for their local equilibrium  
554 concentrations are valid, including the HO<sub>x</sub> – O<sub>x</sub> chemistry only. These conditions describes describe the  
555 HO<sub>2</sub> and OH equilibrium from the top to the some lower borders boundaries, the altitude position of  
556 which vary in the interval between 73 and 85 km and depends essentially on the season and latitude. We  
557 proposed analytical criteria, which almost everywhere well reproduces quite well the main features of  
558 these borders boundaries. Due to weak sensitivity to uncertainties of reaction rates and variables, these  
559 criteria can be considered a robust instrument for HO<sub>2</sub> and OH equilibrium validation. The obtained  
560 results allow extending the abilities of the Panka et al. (2021) method of retrieval of to retrieve  
561 unmeasured components from SABER data. The simultaneous application of OH and HO<sub>2</sub> equilibrium  
562 conditions to the SABER data (O<sub>3</sub>, volume emission rates at 2.0 and 1.6 μm) together with the OH and  
563 HO<sub>2</sub> criteria (16) and (24) to control this equilibrium validity is going allows us to retrieve all unknown  
564 HO<sub>x</sub> – O<sub>x</sub> components (O, H, OH, and HO<sub>2</sub>), extending) and to extend the altitude range of retrieval  
565 downward below 80 km and without external information.

567 **Data availability.** ~~The Panka et al.~~CMAM data are obtained from the ~~SABER~~ website  
568 (~~https://saber.gats-inc.com~~).climate-modelling.canada.ca/climatemodeldata/cmam/cmam30/, last access:  
569 18 May 2024).

570  
571 **Code availability.** Code is available upon request.

572  
573 **Author contributions.** ~~Conceptualization: MK and MB carried out the data processing and analysis and~~  
574 ~~wrote the manuscript.~~ AC, SD, and AM contributed to reviewing the article. AF. Methodology: MK, AF.  
575 Investigation: MK, MB, AC, SD. Software: MB, AC. Visualization: MB, AC. Funding Acquisition: MK.  
576 Writing – original draft preparation: MK, MB. Writing – review & editing: AC, SD. Supervising: AF.

577  
578 **Competing interests.** The authors declare ~~that they have~~ no conflict of interest.

579  
580 **Acknowledgements.** The paper is in the memory of Prof. G.M. Fraiman. The authors are grateful to  
581 reviewers for providing valuable recommendations to improve the paper.

582  
583 **Financial support.** ~~This work was supported by~~The main results presented in Sects. 3-6 were obtained  
584 with the support of the Russian Science Foundation under grant No. 22-12-00064  
585 (~~https://rscf.ru/project/22-12-00064/~~) and/, last access: 18 May 2024). The analysis in Discussion was  
586 carried out at the expense of state assignment ~~no~~No. 0729-2020-0037.

587  
588 **Supplement link:**

589  
590 **References**

591 Avallone, L. M. and Toohey, D. W.: Tests of halogen photochemistry using in situ measurements of ClO  
592 and BrO in the lower polar stratosphere, J. Geophys. Res., 106, 10411–1042,  
593 https://doi.org/10.1029/2000JD900831, 2001.

594 Belikovich, M. V., Kulikov, M. Yu, Grygalashvyly, M., Sonnemann, G. R., Ermakova, T. S., Nechaev,  
595 A. A., and Feigin, A .M.: Ozone chemical equilibrium in the extended mesopause under the nighttime  
596 conditions, Adv. Space Res., 61, 426–432, <https://doi.org/10.1016/j.asr.2017.10.010>, 2018.

597 Berger, U., and U. von Zahn (1999), Two level structure of the mesopause: A model study, *J. Geophys.*  
598 *Res.*, 104, 22,083–22,093.

599 ~~Brooke, J. S., Bernath, P. F., Western, C. M., Sneden, C., Afşar, M., Li, G., and Gordon, I. E.: Line~~  
600 ~~strengths of rovibrational and rotational transitions in the X<sup>2</sup>Π ground state of OH, *Journal of Quantitative*~~  
601 ~~*Spectroscopy and Radiative Transfer*, 168, 142–157, <https://doi.org/10.1016/j.jqsrt.2015.07.021>, 2016.~~

602 Burkholder, J. B., Sander, S. P., Abbatt, J., Barker, J. R., Cappa, C., Crouse, J. D., Dibble, T. S., Huie,  
603 R. E., Kolb, C. E., Kurylo, M. J., Orkin, V. L., Percival, C. J., Wilmouth, D. M., and Wine, P. H.:  
604 Chemical Kinetics and Photochemical Data for Use in Atmospheric Studies, Evaluation No. 19, JPL  
605 Publication 19-5, Jet Propulsion Laboratory, Pasadena, <http://jpldataeval.jpl.nasa.gov>, 2020.

606 ~~Cantrell, C. A., Mauldin, L., Zondlo, M., Eisele, F., Kosciuch, E., Shetter, R., Lefer, B., Hall, S., Campos,~~  
607 ~~T., Ridley, B., Walega, J., Fried, A., Wert, B., Flocke, F., Weinheimer, A., Hannigan, J., Coffey, M.,~~  
608 ~~Atlas, E., Stephens, S., Heikes, B., Snow, J., Blake, D., Blake, N., Katzenstein, A., Lopez, J., Browell, E.~~  
609 ~~V., Dibb, J., Scheuer, E., Seid, G., and Talbot, R.: Steady state free radical budgets and ozone~~  
610 ~~photochemistry during TOPSE, *J. Geophys. Res.*, 108, TOP9-1–TOP9-22,~~  
611 ~~<https://doi.org/10.1029/2002JD002198>, 2003.~~

612 Evans, W. F. J., and Llewellyn, E. J.: Atomic hydrogen concentrations in the mesosphere and the  
613 hydroxyl emissions, *J. Geophys. Res.*, 78, 323–326, <https://doi.org/10.1029/JA078i001p00323>, 1973.

614 Evans, W. F. J., McDade, I. C., Yuen, J., and Llewellyn, E. J.: A rocket measurement of the O<sub>2</sub> infrared  
615 atmospheric (0-0) band emission in the dayglow and a determination of the mesospheric ozone and  
616 atomic oxygen densities, *Can. J. Phys.*, 66, 941–946, <https://doi.org/10.1139/p88-151>. 1988.

617 Fytterer, T., von Savigny, C., Mlynčzak, M., and Sinnhuber, M.: Model results of OH airglow  
618 considering four different wavelength regions to derive night-time atomic oxygen and atomic hydrogen in  
619 the mesopause region, *Atmos. Chem. Phys.*, 19, 1835–1851, <https://doi.org/10.5194/acp-19-1835-2019>,  
620 2019.

621 Good, R. E.: Determination of atomic oxygen density from rocket borne measurements of hydroxyl  
622 airglow, *Planet. Space Sci.*, 24, 389–395, [https://doi.org/10.1016/0032-0633\(76\)90052-0](https://doi.org/10.1016/0032-0633(76)90052-0), 1976.

623 Grygalashvyly, M., Sonnemann, G. R., and Hartogh, P.: Long-term behavior of the concentration of the  
624 minor constituents in the mesosphere - ~~Aa~~ model study, *Atmos. Chem. Phys.*, 9, 2779–2792,  
625 <https://doi.org/10.5194/acp-9-2779-2009>, 2009.

626 Grygalashvyly, M., Sonnemann, G. R., Lübken, F.-J., Hartogh, P., and Berger, U.: Hydroxyl layer: Mean  
627 state and trends at midlatitudes, *J. Geophys. Res. Atmos.*, 119, 12,391–12,419,  
628 <https://doi.org/10.1002/2014JD022094>, 2014.

629 Grygalashvyly, M.: Several notes on the OH\* layer, *Ann. Geophys.*, 33, 923-930,  
630 <https://doi.org/10.5194/angeo-33-923-2015>, 2015.

631 Hartogh, P., Jarchow, C., Sonnemann, G. R., and Grygalashvyly, M.: On the spatiotemporal behavior of  
632 ozone within the upper mesosphere/mesopause region under nearly polar night conditions, *J. Geophys.*  
633 *Res.*, 109, D18303, <https://doi.org/10.1029/2004JD004576>, 2004.

634 Hartogh, P., Jarchow, Ch., Sonnemann, G. R., and Grygalashvyly, M.: Ozone distribution in the middle  
635 latitude mesosphere as derived from microwave measurements at Lindau (51.66°N, 10.13°E), *J. Geophys.*  
636 *Res.*, 116, D04305, <https://doi.org/10.1029/2010JD014393>, 2011.

637 Körner, U., and Sonnemann, G. R.: Global 3D-modeling of water vapor concentration of the  
638 mesosphere/mesopause region and implications with respect to the NLC region, *J. Geophys. Res.*, 106,  
639 9639–9651, <https://doi.org/10.1029/2000JD900744>, 2001.

640 Kowalewski, S., v. Savigny, C., Palm, M., McDade, I. C., and Notholt, J.: On the impact of the temporal  
641 variability of the collisional quenching process on the mesospheric OH emission layer: a study based on  
642 SD-WACCM4 and SABER, *Atmos. Chem. Phys.*, 14, 10193-10210, [https://doi.org/10.5194/acp-14-](https://doi.org/10.5194/acp-14-10193-2014)  
643 10193-2014, 2014.

644 Kremp, C., Berger, U., Hoffmann, P., Keuer, D., and Sonnemann, G. R.: Seasonal variation of middle  
645 latitude wind fields of the mesopause region—A comparison between observation and model calculation,  
646 *Geophys. Res. Lett.*, 26, 1279–1282, <https://doi.org/10.1029/1999GL900218>, 1999.

647 Kulikov, M. Y., Feigin, A. M., and Sonnemann, G. R.: Retrieval of the vertical distribution of chemical  
648 components in the mesosphere from simultaneous measurements of ozone and hydroxyl distributions,  
649 *Radiophys. Quantum Electron.*, 49, 683–691, <https://doi.org/10.1007/s11141-006-0103-4>, 2006.

650 Kulikov, M. Yu., Feigin, A. M., and Sonnemann, G. R.: Retrieval of water vapor profile in the  
651 mesosphere from satellite ozone and hydroxyl measurements by the basic dynamic model of mesospheric  
652 photochemical system, *Atmos. Chem. Phys.*, 9, 8199–8210, <https://doi.org/10.5194/acp-9-8199-2009>,  
653 2009.

654 Kulikov, M. Y., Belikovich, M. V., Grygalashvyly, M., Sonnemann, G. R., Ermakova, T. S., Nechaev, A.  
655 A., and Feigin, A. M.: Daytime ozone loss term in the mesopause region, *Ann. Geophys.*, 35, 677-682  
656 <https://doi.org/10.5194/angeo-35-677-2017>, 2017.

657 Kulikov, M. Y., Nechaev, A. A., Belikovich, M. V., Ermakova, T. S., and Feigin, A. M.: Technical note:  
658 Evaluation of the simultaneous measurements of mesospheric OH, HO<sub>2</sub>, and O<sub>3</sub> under a photochemical  
659 equilibrium assumption – a statistical approach, *Atm. Chem. Phys.*, 18, 7453-747,  
660 <https://doi.org/10.5194/acp-18-7453-2018>, 2018a.

661 Kulikov, M. Y., Belikovich, M. V., Grygalashvyly, M., Sonnemann, G. R., Ermakova, T. S., Nechaev, A.  
662 A., and Feigin, A. M.: Nighttime ozone chemical equilibrium in the mesopause region. *J. Geophys.*  
663 *Res.*, 123, 3228–3242, <https://doi.org/10.1002/2017JD026717>, 2018b.

664 Kulikov, M. Yu., Nechaev, A. A., Belikovich, M. V., Vorobeva, E. V., Grygalashvyly, M., Sonnemann,  
665 G. R., and Feigin, A. M.: Border of nighttime ozone chemical equilibrium in the mesopause region from

666 | [saber](#)**SABER** data: implications for derivation of atomic oxygen and atomic hydrogen, *Geophys. Res. Lett.*, 46, 997–1004, <https://doi.org/10.1029/2018GL080364>, 2019.

667

668 Kulikov, M. Y., Belikovich, M. V., Feigin, A. M.: The 2-day photochemical oscillations in the mesopause  
669 region: the first experimental evidence? *Geophys. Res. Lett.*, 48, e2021GL092795,  
670 <https://doi.org/10.1029/2021GL092795>, 2021.

671 Kulikov M.Yu., Belikovich, M.V., Grygalashvyly, M., Sonnemann, G. R., and Feigin, A.M.: Retrieving  
672 daytime distributions of O, H, OH, HO<sub>2</sub>, and chemical heating rate in the mesopause region from satellite  
673 observations of ozone and OH\* volume emission: The evaluation of the importance of the reaction  
674  $H+O_3 \rightarrow O_2+OH$  in the ozone balance, *Adv. Space Res.*, 69(9), 3362-3373,  
675 <https://doi.org/10.1016/j.asr.2022.02.011>, 2022a.

676 Kulikov, M. Y., Belikovich, M. V., Grygalashvyly, M., Sonnemann, G. R., and Feigin, A.M.: The revised  
677 method for retrieving daytime distributions of atomic oxygen and odd-hydrogens in the mesopause region  
678 from satellite observations, *Earth, Planets and Space*, 74, 44, [https://doi.org/10.1186/s40623-022-01603-](https://doi.org/10.1186/s40623-022-01603-8)  
679 8, 2022b.

680 Kulikov, M. Yu., Belikovich, M. V., Chubarov, A. G., Dementeyva, S. O., Feigin, A. M.: Boundary of  
681 nighttime ozone chemical equilibrium in the mesopause region: improved criterion of determining the  
682 boundary from satellite data, *Adv. Space Res.*, 71 (6), 2770-2780,  
683 <https://doi.org/10.1016/j.asr.2022.11.005>, 2023a.

684 Kulikov, M. Yu., Belikovich, M. V., Chubarov, A. G., Dementyeva, S. O., and Feigin, A. M.: Boundary  
685 of nighttime ozone chemical equilibrium in the mesopause region: long-term evolution determined using  
686 20-year satellite observations, *Atmos. Chem. Phys.*, 23, 14593–14608, [https://doi.org/10.5194/acp-23-](https://doi.org/10.5194/acp-23-14593-2023)  
687 14593-2023, 2023b.

688 Llewellyn, E. J., McDade, I. C. Moorhouse, P. and Lockerbie M. D.: Possible reference models for  
689 atomic oxygen in the terrestrial atmosphere, *Adv. Space Res.*, 13, 135–144, [https://doi.org/10.1016/0273-](https://doi.org/10.1016/0273-1177(93)90013-2)  
690 1177(93)90013-2, 1993.

691 Llewellyn, E. J., and McDade, I. C.: A reference model for atomic oxygen in the terrestrial atmosphere,  
692 *Adv. Space Res.*, 18, 209–226, [https://doi.org/10.1016/0273-1177\(96\)00059-2](https://doi.org/10.1016/0273-1177(96)00059-2), 1996.

693 Manney, G. L., Kruger, K., Sabutis, J. L., Sena, S. A., and Pawson, S.: The remarkable 2003–2004 winter  
694 and other recent warm winters in the Arctic stratosphere since the late 1990s. *J. Geophys. Res.*, 110,  
695 D04107, <https://doi.org/10.1029/2004JD005367>, 2005.

696 | [Marchand, M., Bekki, S., Lefevre, F., and Hauchecorne, A.: Temperature retrieval from stratospheric O3  
697 and NO3 GOMOS data, \*Geophys. Res. Lett.\*, 34, L24809, <https://doi.org/10.1029/2007GL030280>, 2007.](#)

698 Marsh, D. R., Smith, A. K., Mlynczak, M. G., and Russell III, J. M.: SABER observations of the OH  
699 Meinel airglow variability near the mesopause, *J. Geophys. Res.*, 111, A10S05,  
700 <https://doi.org/10.1029/2005JA011451>, 2006.

701 McDade, I. C., Llewellyn, E. J., and Harris, F. R.: Atomic oxygen concentrations in the lower auroral  
702 thermosphere, *Adv. Space Res.*, 5, 229–232, <https://doi.org/10.1029/GL011I003P00247>, 1985.

703 McDade, I. C., and Llewellyn, E. J.: Mesospheric oxygen atom densities inferred from night-time OH  
704 Meinel band emission rates, *Planet. Space Sci.*, 36, 897–905, [https://doi.org/10.1016/0032-](https://doi.org/10.1016/0032-0633(88)90097-9)  
705 [0633\(88\)90097-9](https://doi.org/10.1016/0032-0633(88)90097-9), 1988.

706 Mlynczak, M. G., Marshall, B. T., Martin-Torres, F. J., Russell III, J. M., Thompson, R. E., Remsberg, E.  
707 E., and Gordley, L. L.: Sounding of the Atmosphere using Broadband Emission Radiometry observations  
708 of daytime mesospheric O<sub>2</sub>(<sup>1</sup>D) 1.27 μm emission and derivation of ozone, atomic oxygen, and solar and  
709 chemical energy deposition rates, *J. Geophys. Res.*, 112, D15306, <https://doi.org/10.1029/2006JD008355>,  
710 2007.

711 Mlynczak, M. G., Hunt, L. A., Mast, J. C., Marshall, B. T., Russell III, J. M., Smith, A. K., Siskind, D. E.,  
712 Yee, J.-H., Mertens, C. J., Martin-Torres, F. J., Thompson, R. E., Drob, D. P., and Gordley, L. L.: Atomic  
713 oxygen in the mesosphere and lower thermosphere derived from SABER: Algorithm theoretical basis and  
714 measurement uncertainty, *J. Geophys. Res.*, 118, 5724–5735, <https://doi.org/10.1002/jgrd.50401>, 2013a.

715 Mlynczak, M. G., Hunt, L. H., Mertens, C. J., Marshall, B. T., Russell III, J. M., López-Puertas, M.,  
716 Smith, A. K., Siskind, D. E., Mast, J. C., Thompson, R. E., and Gordley, L. L.: Radiative and energetic  
717 constraints on the global annual mean atomic oxygen concentration in the mesopause region, *J. Geophys.*  
718 *Res. Atmos.*, 118, 5796–5802, <https://doi.org/10.1002/jgrd.50400>, 2013b.

719 Mlynczak, M. G., Hunt, L. A. Marshall, B. T. Mertens, C. J. Marsh, D. R. Smith, A. K. Russell, J. M.  
720 Siskind D. E., and Gordley L. L.: Atomic hydrogen in the mesopause region derived from SABER:  
721 Algorithm theoretical basis, measurement uncertainty, and results, *J. Geophys. Res.*, 119, 3516–3526,  
722 <https://doi.org/10.1002/2013JD021263>, 2014.

723 Mlynczak, M. G., Hunt, L. A., Russell, J. M. III, and Marshall, B. T.: Updated SABER night atomic  
724 oxygen and implications for SABER ozone and atomic hydrogen, *Geophys. Res. Lett.*, 45, 5735–5741,  
725 <https://doi.org/10.1029/2018GL077377>, 2018.

726 Morton, K. W., and Mayers, D. F.; *Numerical Solution of Partial Differential Equations*, Cambridge  
727 University Press, 1994.

728 Nikoukar, R., Swenson, G. R., Liu, A. Z., and Kamalabadi, F.: On the variability of mesospheric OH  
729 emission profiles, *J. Geophys. Res.*, 112, D19109, <https://doi.org/10.1029/2007JD008601>, 2007.

730 Panka, P. A., Kutepov, A. A., Zhu, Y., Kaufmann, M., Kalogerakis, K. S., Rezac, L., et al.: Simultaneous  
731 retrievals of nighttime O(<sup>3</sup>P) and total OH densities from satellite observations of Meinel band emissions.  
732 *Geoph. Res.Lett.*, 48, e2020GL091053, <https://doi.org/10.1029/2020GL091053>, 2021.

733 Pendleton, W. R., Baker, K. D., Howlett, L. C.: Rocket-based investigations of O(<sup>3</sup>P), O<sub>2</sub> (a<sup>1</sup>Δ<sub>g</sub>) and OH\*  
734 (v=1,2) during the solar eclipse of 26 February 1979, *J. Atm. Terr. Phys.*, 45(7), 479-491, 1983.



735 Siskind, D. E., Marsh, D. R., Mlynczak, M. G., Martin-Torres, F. J., and Russell III, J. M.: Decreases in  
736 atomic hydrogen over the summer pole: Evidence for dehydration from polar mesospheric clouds?  
737 *Geophys. Res. Lett.*, 35, L13809, <https://doi.org/10.1029/2008GL033742>, 2008.

738 Russell, J. P., and Lowe, R. P.: Atomic oxygen profiles (80-94 km) derived from Wind Imaging  
739 Interferometer/Upper Atmospheric Research Satellite measurements of the hydroxyl airglow: 1.  
740 Validation of technique, *J. Geophys. Res.*, 108(D21), 4662, <https://doi.org/10.1029/2003JD003454>, 2003.

741 Russell, J. P., Ward, W. E., Lowe, R. P., Roble, R. G., Shepherd, G. G., and Solheim, B.: Atomic oxygen  
742 profiles (80 to 115 km) derived from Wind Imaging Interferometer/Upper Atmospheric Research Satellite  
743 measurements of the hydroxyl and green line airglow: Local time–latitude dependence, *J. Geophys. Res.*,  
744 110(D15), D15305, <https://doi.org/10.1029/2004JD005570>, 2005.

745 Siskind, D. E., Mlynczak, M. G., Marshall, T., Friedrich, M., Gumbel, J.: Implications of odd oxygen  
746 observations by the TIMED/SABER instrument for lower D region ionospheric modeling, *J. Atmos. Sol.*  
747 *Terr. Phys.*, 124, 63–70, <https://doi.org/10.1016/j.jastp.2015.01.014>, 2015.

748 Smith, A. K., Lopez-Puertas, M., Garcia-Comas, M. and Tukiainen, S.: SABER observations of  
749 mesospheric ozone during NH late winter 2002–2009, *Geophys. Res. Lett.*, 36, L23804,  
750 <https://doi.org/10.1029/2009GL040942>, 2009.

751 Smith, A. K., Marsh, D. R. Mlynczak, M. G. and Mast, J. C.: Temporal variations of atomic oxygen in the  
752 upper mesosphere from SABER, *J. Geophys. Res.*, 115, D18309, <https://doi.org/10.1029/2009JD013434>,  
753 2010.

754 [Scinocca, J. F., McFarlane, N. A., Lazare, M., Li, J., and Plummer, D.: The CCCma third generation](#)  
755 [AGCM and its extension into the middle atmosphere, \*Atmos. Chem. Phys.\*, 8, 7055–7074,](#)  
756 [<https://doi.org/10.5194/acp-8-7055-2008>, 2008.](#)

757 Sonnemann, G., Kremp, C. Ebel, A. and Berger U.: A three-dimensional dynamic model of minor  
758 constituents of the mesosphere, *Atmos. Environ.*, 32, 3157–3172, [https://doi.org/10.1016/S1352-](https://doi.org/10.1016/S1352-2310(98)00113-7)  
759 2310(98)00113-7, 1998.

760 Sonnemann, G. R., Grygalashvyly, M., Hartogh, P., and Jarchow, C.: Behavior of mesospheric ozone  
761 under nearly polar night conditions, *Adv. Space Res.*, 38, 2402–2407,  
762 <https://doi.org/10.1016/j.asr.2006.09.011>, 2006.

763 Sonnemann, G. R., Hartogh, P., Grygalashvyly, M., Li, S., and Berger, U.: The quasi 5-day signal in the  
764 mesospheric water vapor concentration at high latitudes in 2003-a comparison between observations at  
765 ALOMAR and calculations, *J. Geophys. Res.*, 113, D04101, <https://doi.org/10.1029/2007JD008875>,  
766 2008.

767 Sonnemann, G. R., Hartogh, P., Berger, U., and Grygalashvyly, M.: Hydroxyl layer: trend of number  
768 density and intra-annual variability, *Ann. Geophys.*, 33, 749–767, [https://doi.org/10.5194/angeo-33-749-](https://doi.org/10.5194/angeo-33-749-2015)  
769 2015, 2015.

770 | [Stedman, D. H., Chameides, W., and Jackson, J. O.: Comparison of experimental and computed values](#)  
771 | [for J\(NO<sub>2</sub>\), Geophys. Res. Lett., 2, 22–25, <https://doi.org/10.1029/GL002i001p00022>, 1975.](#)

772 Swenson, G. R., and Gardner C. S.: Analytical models for the responses of the mesospheric OH\* and Na  
773 layers to atmospheric gravity waves, J. Geophys. Res., 103(D6), 6271–6294,  
774 <https://doi.org/10.1029/97JD02985>, 1998.

775 Thomas, R. J.: Atomic hydrogen and atomic oxygen density in the mesosphere region: Global and  
776 seasonal variations deduced from Solar Mesosphere Explorer near-infrared emissions, J. Geophys. Res.,  
777 95, 16,457–16,476, <https://doi.org/10.1029/JD095iD10p16457>, 1990.

778 Walcek, C. J.: Minor flux adjustment near mixing ratio extremes for simplified yet highly accurate  
779 monotonic calculation of tracer advection, J. Geophys. Res., 105, 9335-9348,  
780 <https://doi.org/10.1029/1999JD901142>, 2000.

781 Xu, J., Smith, A. K., Jiang, G., Gao, H., Wei, Y., Mlynczak, M. G., and Russell III, J. M.: Strong  
782 longitudinal variations in the OH nightglow, Geophys. Res. Lett., 37, L21801,  
783 <https://doi.org/10.1029/2010GL043972>, 2010.

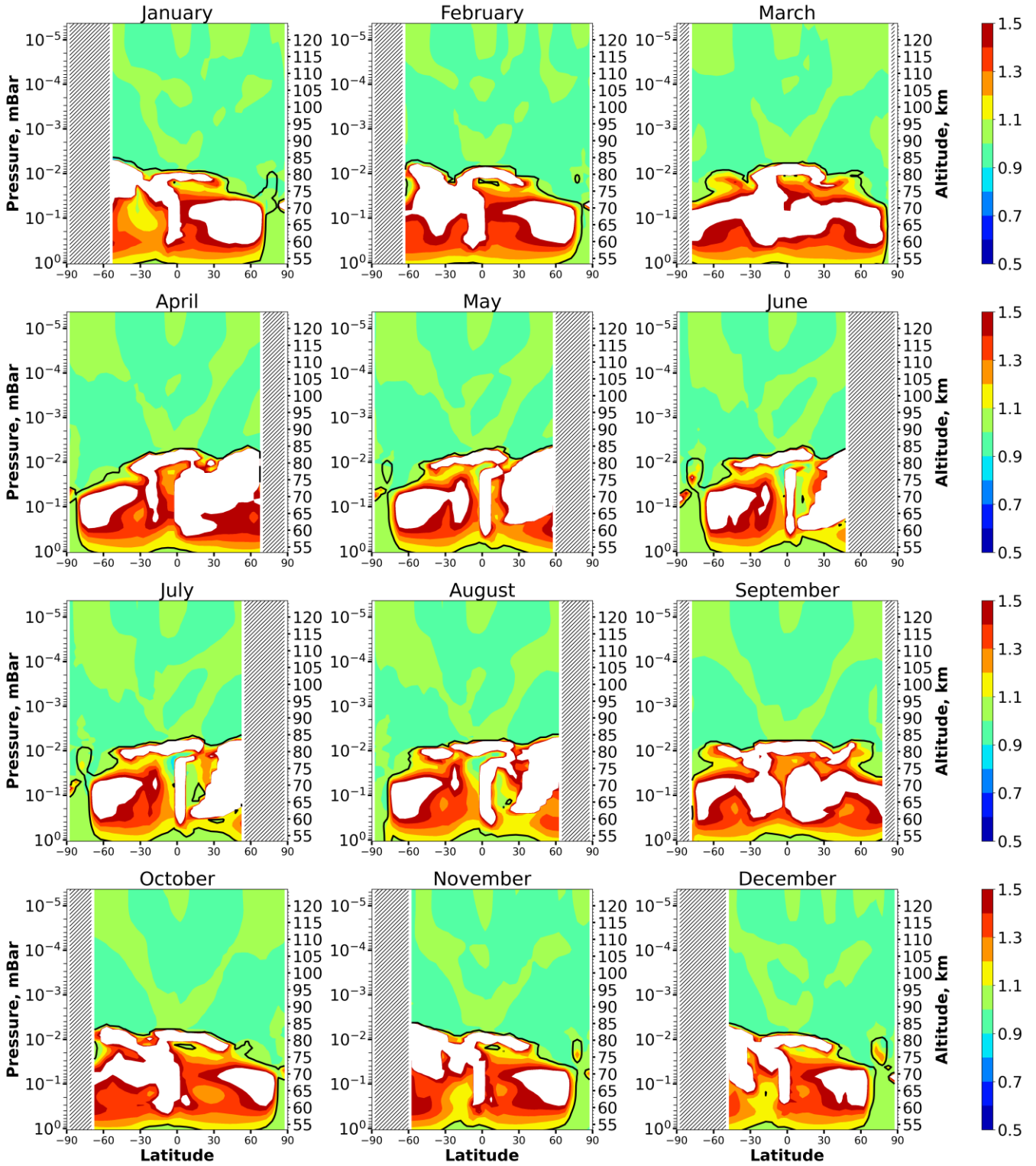
784 Xu, J., Gao, H. Smith, A. K. and Zhu Y.: Using TIMED/SABER nightglow observations to investigate  
785 hydroxyl emission mechanisms in the mesopause region, J. Geophys. Res., 117, D02301,  
786 <https://doi.org/10.1029/2011JD016342>, 2012.

787 **Table 1.** List of reactions included in 3-d chemical transport model with the corresponding reaction rates  
 788 taken from Burkholder et al. (2020).

1	$O(^1D)+O_2 \rightarrow O+O_2$	24	$H+OH+N_2 \rightarrow H_2O+N_2$	47	$NO+O_3 \rightarrow NO_2+O_2$
2	$O(^1D)+N_2 \rightarrow O+N_2$	25	$OH+H_2 \rightarrow H_2O+H$	48	$NO_2+O_3 \rightarrow NO_3+O_2$
3	$O(^1D)+O_3 \rightarrow O_2+2O$	26	$OH+OH \rightarrow H_2O+O$	49	$N+OH \rightarrow NO+H$
4	$O(^1D)+O_3 \rightarrow 2O_2$	27	$OH+OH+M \rightarrow H_2O_2+M$	50	$NO+HO_2 \rightarrow NO_2+OH$
5	$O(^1D)+N_2O \rightarrow 2NO$	28	$OH+HO_2 \rightarrow H_2O+O_2$	51	$H+NO_2 \rightarrow OH+NO$
6	$O(^1D)+N_2O \rightarrow N_2+O_2$	29	$H_2O_2+OH \rightarrow H_2O+HO_2$	52	$NO_3+NO \rightarrow 2NO_2$
7	$O(^1D)+H_2O \rightarrow 2OH$	30	$HO_2+HO_2 \rightarrow H_2O_2+O_2$	53	$N+NO \rightarrow N_2+O$
8	$O(^1D)+H_2 \rightarrow H+OH$	31	$HO_2+HO_2+M \rightarrow H_2O_2+O_2+M$	54	$N+NO_2 \rightarrow N_2O+O$
9	$O(^1D)+CH_4 \rightarrow CH_3+OH$	32	$OH+CO \rightarrow H+CO_2$	55	$O_2+h\nu \rightarrow 2O$
10	$O(^1D)+CH_4 \rightarrow H_2+CH_2O$	33	$CH_4+OH \rightarrow CH_3+H_2O$	56	$O_2+h\nu \rightarrow O+O(^1D)$
11	$O+O+M \rightarrow O_2+M$	34	$CH_3+O_2 \rightarrow CH_3O_2$	57	$O_3+h\nu \rightarrow O_2+O$
12	$O+O_2+M \rightarrow O_3+M$	35	$CH_3+O \rightarrow CH_2O+H$	58	$O_3+h\nu \rightarrow O_2+O(^1D)$
13	$O+O_3 \rightarrow O_2+O_2$	36	$CH_3O_2+NO \rightarrow CH_3O+NO_2$	59	$N_2+h\nu \rightarrow 2N$
14	$H+HO_2 \rightarrow 2OH$	37	$CH_3O+O_2 \rightarrow CH_2O+HO_2$	60	$NO+h\nu \rightarrow N+O$
15	$H+HO_2 \rightarrow H_2O+O$	38	$CH_2O \rightarrow H_2+CO$	61	$NO_2+h\nu \rightarrow NO+O$
16	$H+HO_2 \rightarrow H_2+O_2$	39	$CH_2O \rightarrow H+CHO$	62	$N_2O+h\nu \rightarrow N_2+O(^1D)$
17	$OH+O \rightarrow H+O_2$	40	$CHO+O_2 \rightarrow HO_2+CO$	63	$N_2O+h\nu \rightarrow N+NO$
18	$HO_2+O \rightarrow OH+O_2$	41	$O_3+N \rightarrow NO+O_2$	64	$NO_3+h\nu \rightarrow NO_2+O$
19	$H_2O_2+O \rightarrow OH+HO_2$	42	$NO_3+O \rightarrow NO_2+O_2$	65	$H_2O+h\nu \rightarrow H+OH$
20	$H+O_2+M \rightarrow HO_2+M$	43	$O+NO+M \rightarrow NO_2+M$	66	$H_2O_2+h\nu \rightarrow 2OH$
21	$H+O_3 \rightarrow OH+O_2$	44	$NO_2+O \rightarrow NO+O_2$	67	$CH_4+h\nu \rightarrow CH_2+H_2$
22	$OH+O_3 \rightarrow O_2+HO_2$	45	$NO_2+O+M \rightarrow NO_3+M$	68	$CH_4+h\nu \rightarrow CH+H_2+H$
23	$HO_2+O_3 \rightarrow OH+2O_2$	46	$N+O_2 \rightarrow NO+O$	69	$CO_2+h\nu \rightarrow CO+O$

789

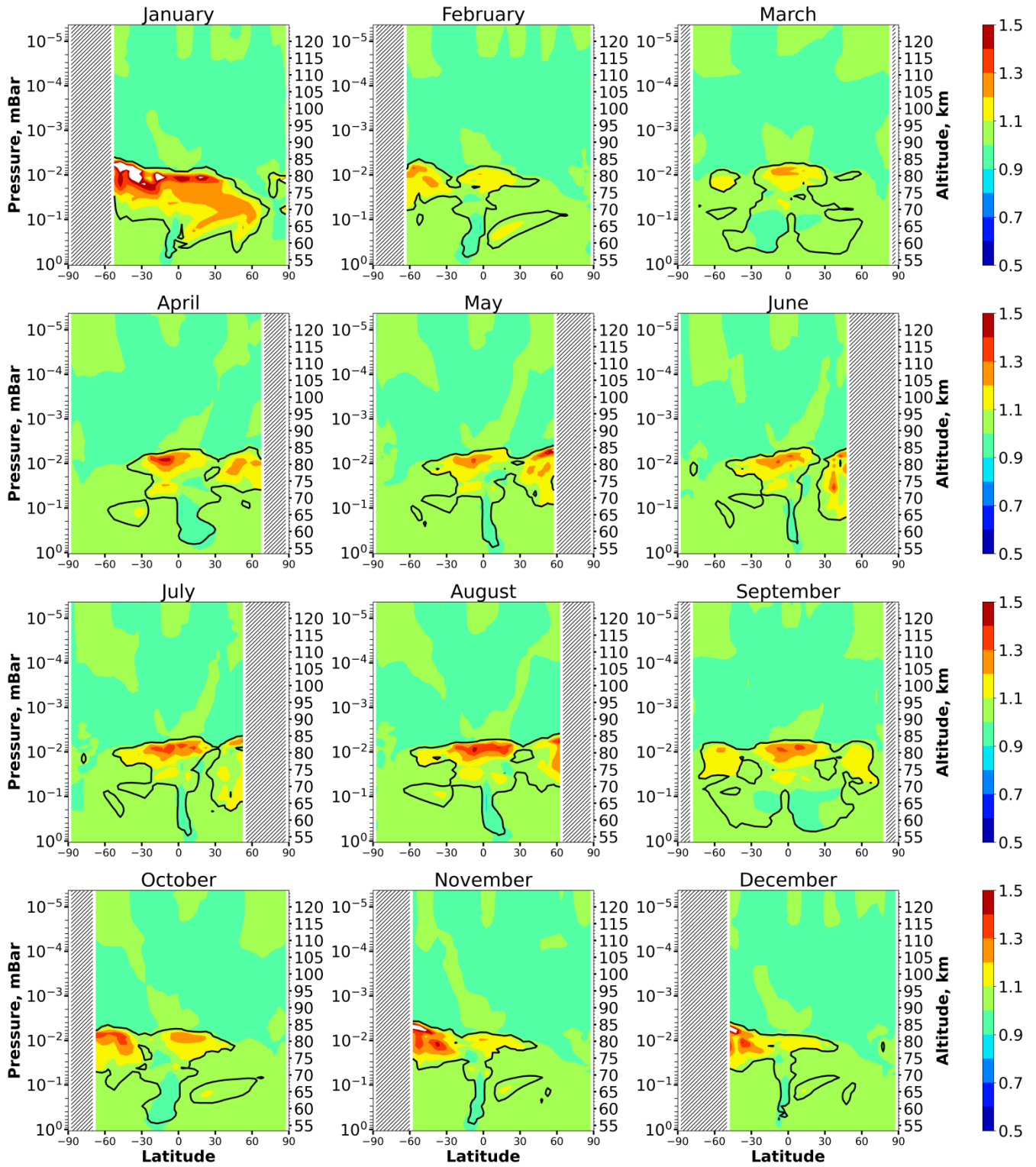
790



791

792 Figure 1. Nighttime mean and monthly averaged  $HO_2/HO_2^{eq}$ , where  $HO_2^{eq}$  is equilibrium concentration  
 793 determined by Eq. (5). Black line shows the borderboundary of  $HO_2$  equilibrium according to condition  
 794 (1). The stippling corresponds to  $\chi < 105^\circ$ . The white area represents the  $< HO_2/HO_2^{eq} >$  ratio outside the  
 795  $[0.5, 1.5]$  interval.

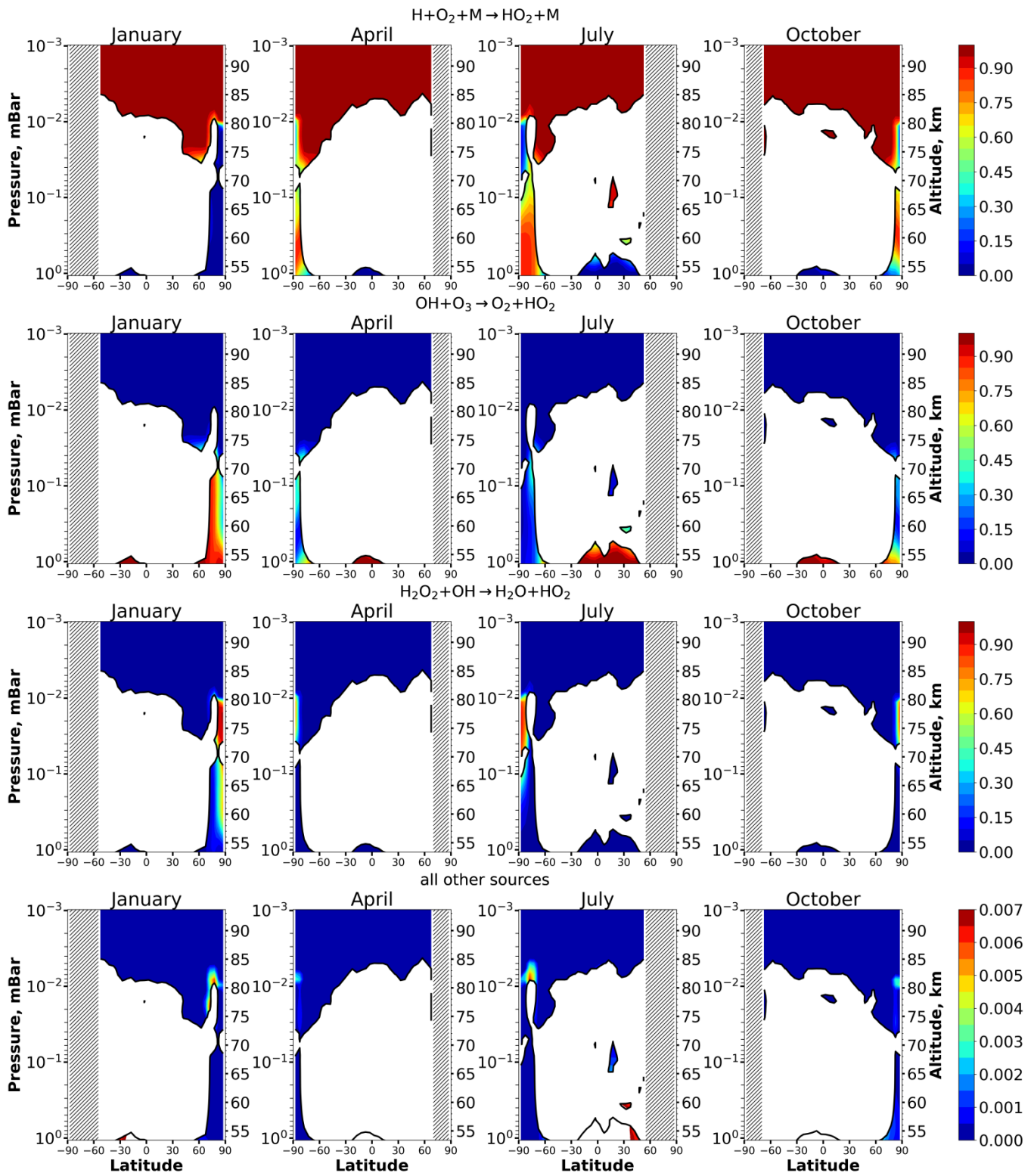
796

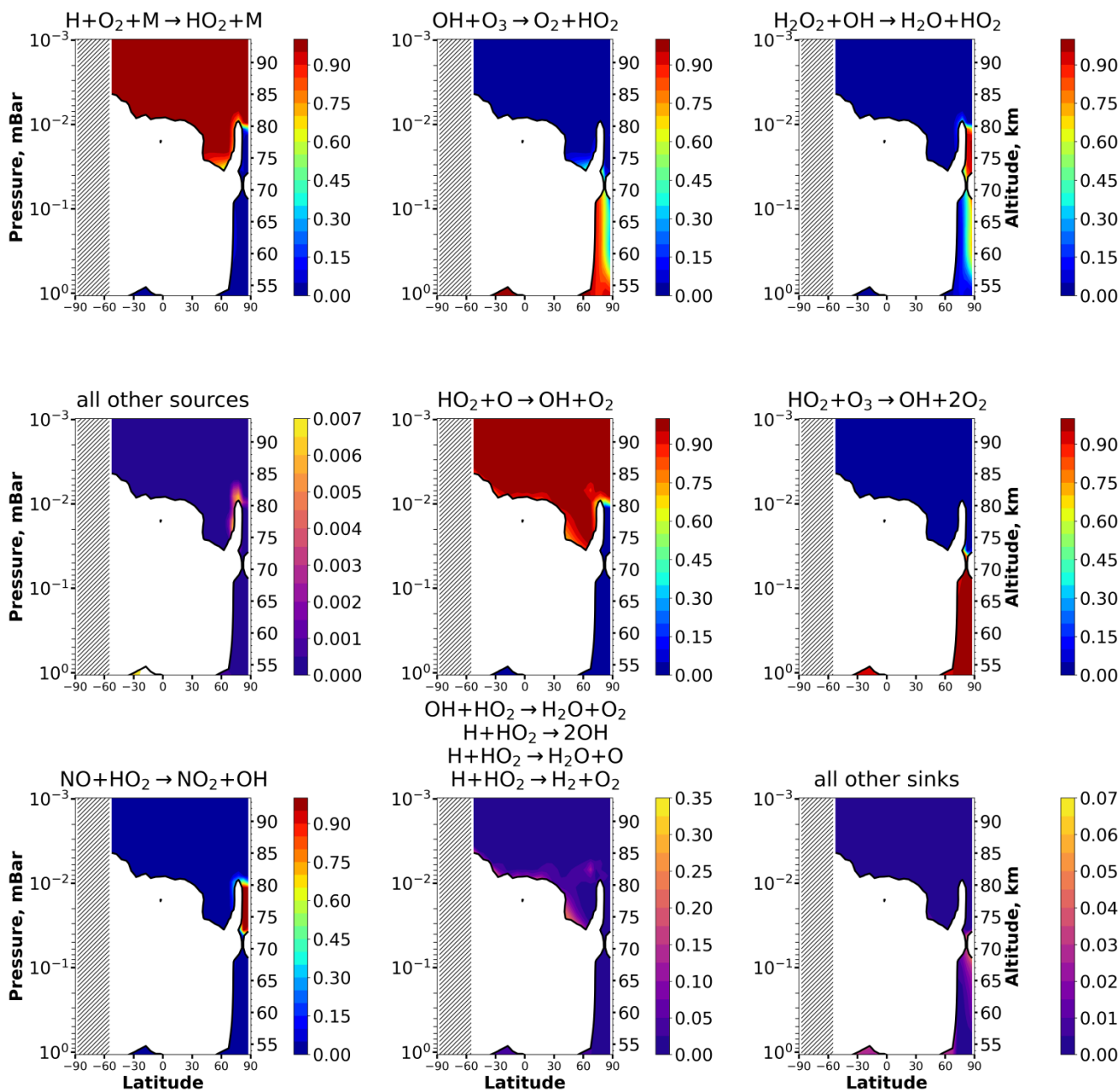


797

798 Figure 2. Nighttime mean and monthly averaged  $OH/OH^{eq}$ , where  $OH^{eq}$  is equilibrium concentration  
 799 determined by Eq. (6). Black line shows the borderboundary of OH equilibrium according to condition  
 800 (1). The stippling corresponds to  $\chi < 105^\circ$ . The white area represents the  $\langle OH/OH^{eq} \rangle$  ratio outside the  
 801  $[0.5, 1.5]$  interval.

802

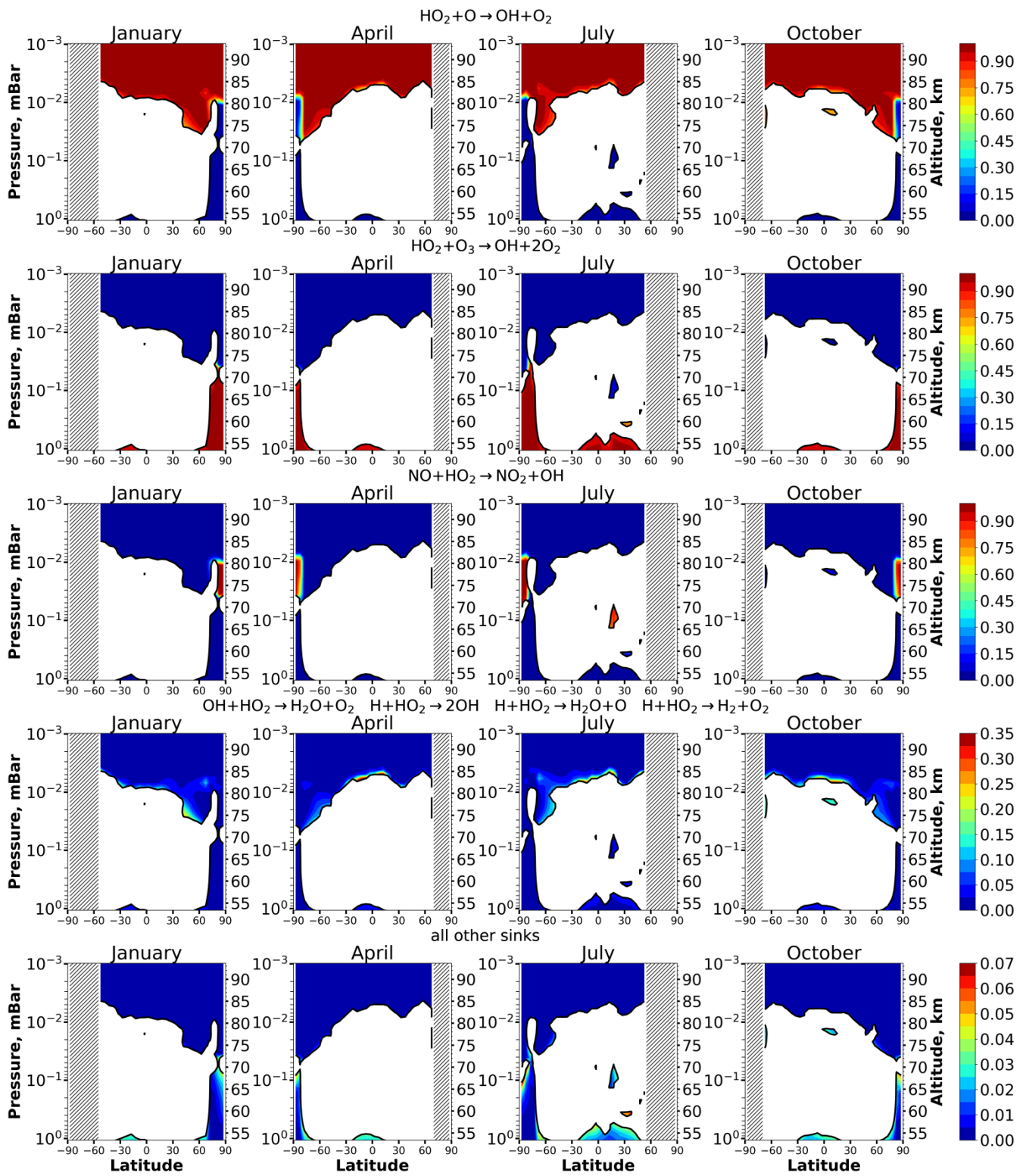




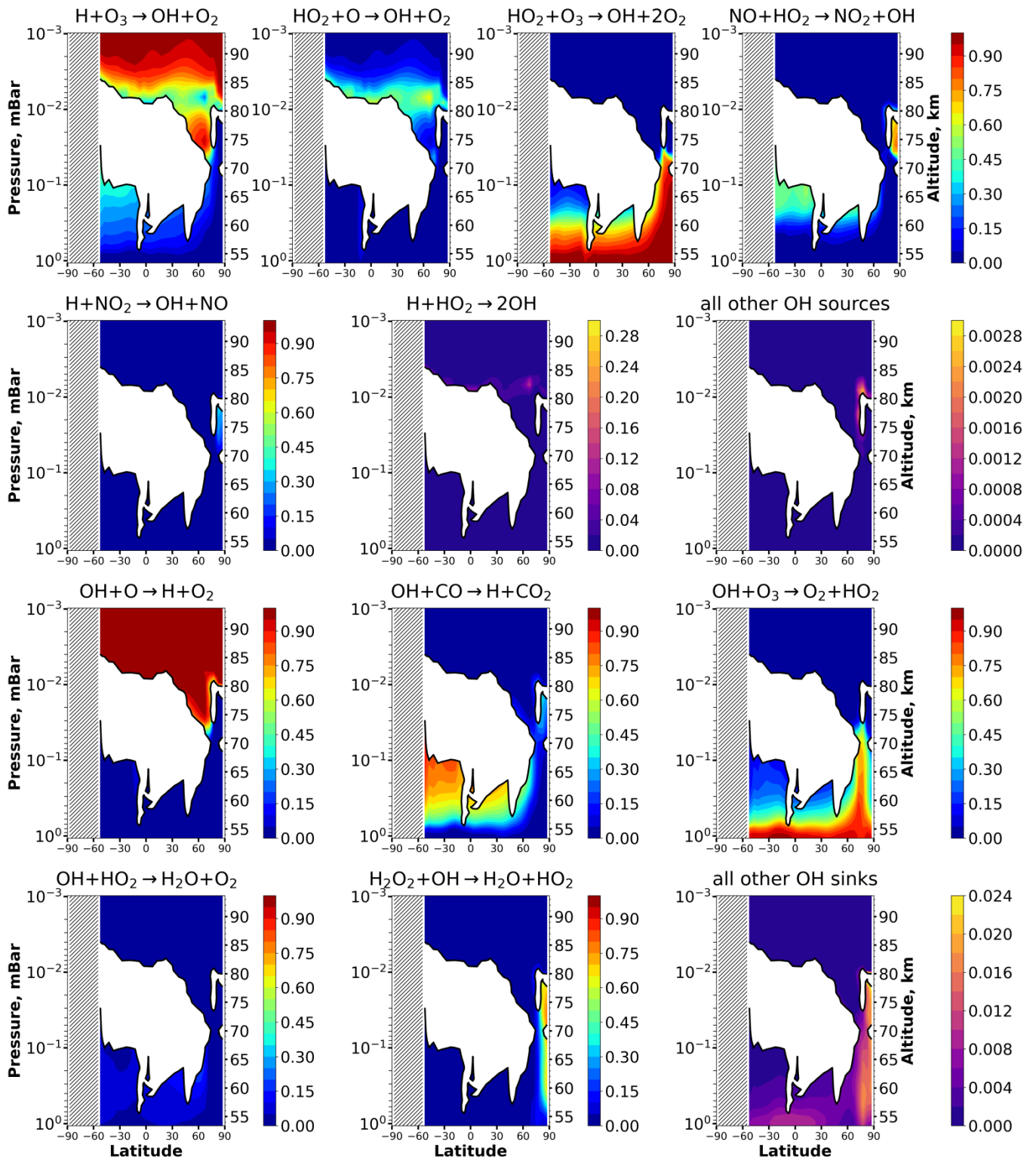
804

805 Figure 3. Nighttime mean and monthly averaged ~~the~~ relative contribution of a certain reaction to the total  
 806 source or sink of HO<sub>2</sub> in equilibrium areas. The stippling corresponds to  $\chi < 105^\circ$ . White color  
 807 points indicates nonequilibrium areas of HO<sub>2</sub>.

808



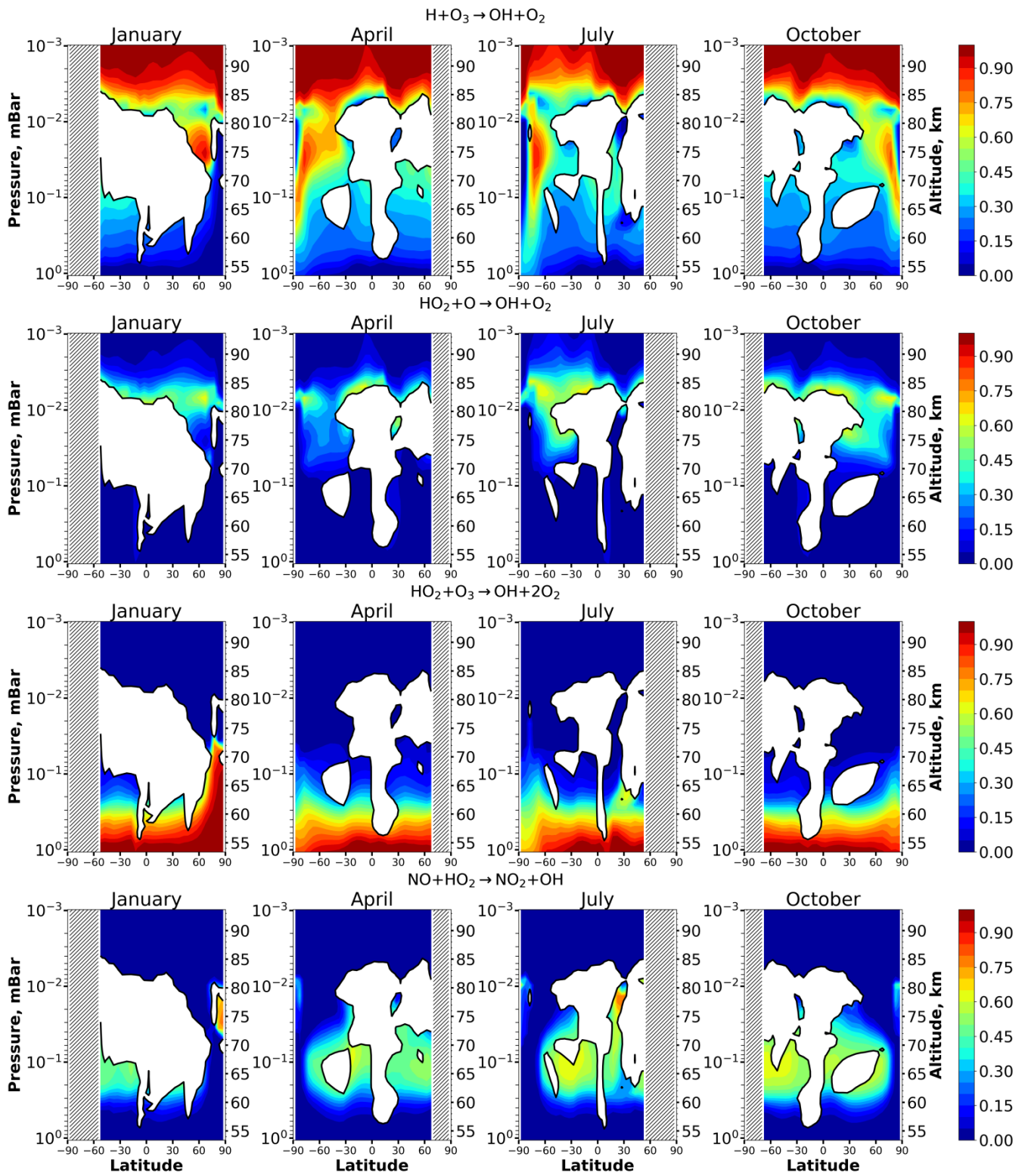




810

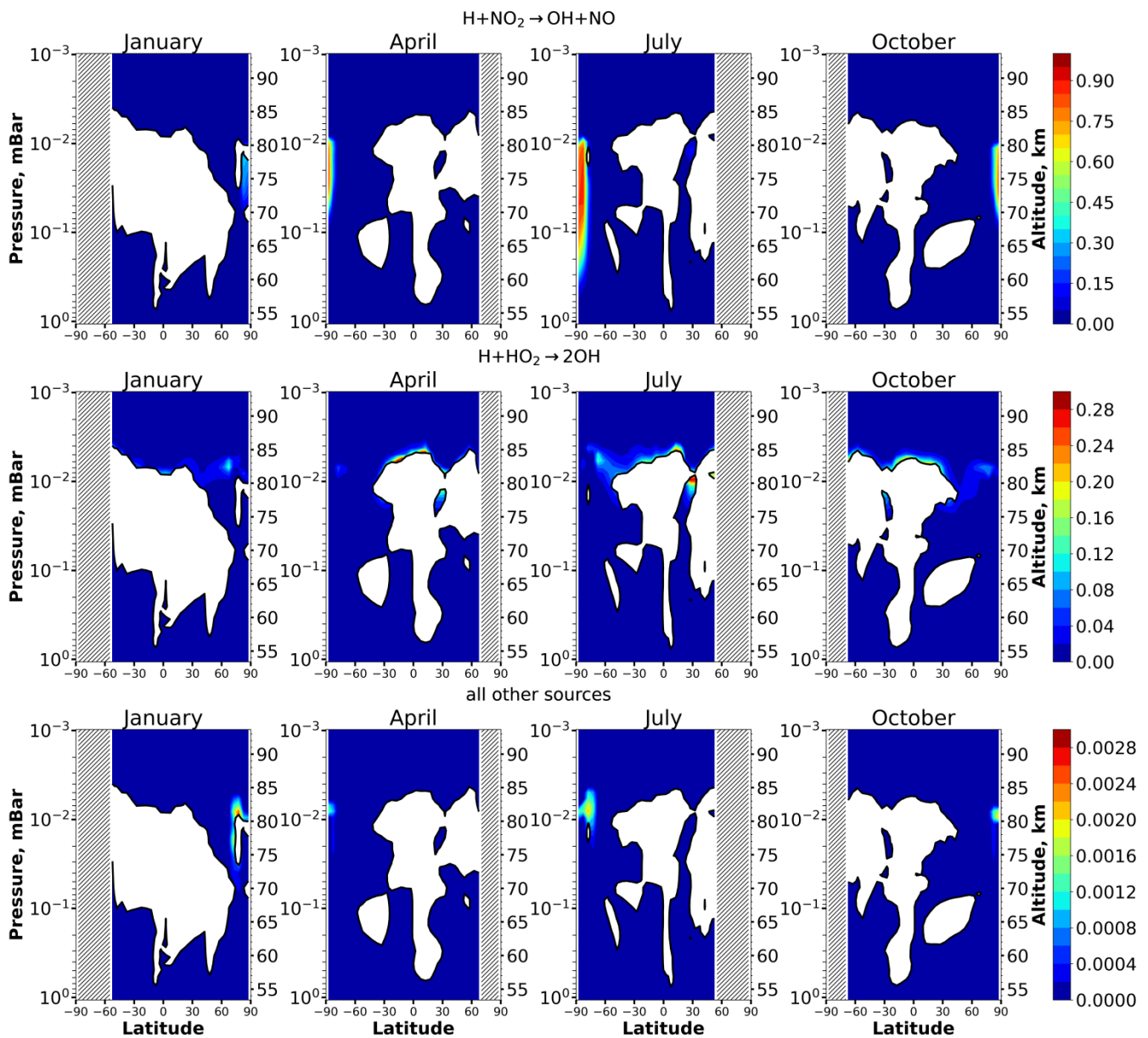
811 Figure 4. Nighttime mean and monthly averaged **the relative contribution of a certain reaction to the total**  
 812 **sink of HO<sub>2</sub> in equilibrium areas. White color points nonequilibrium areas of HO<sub>2</sub>.**

813

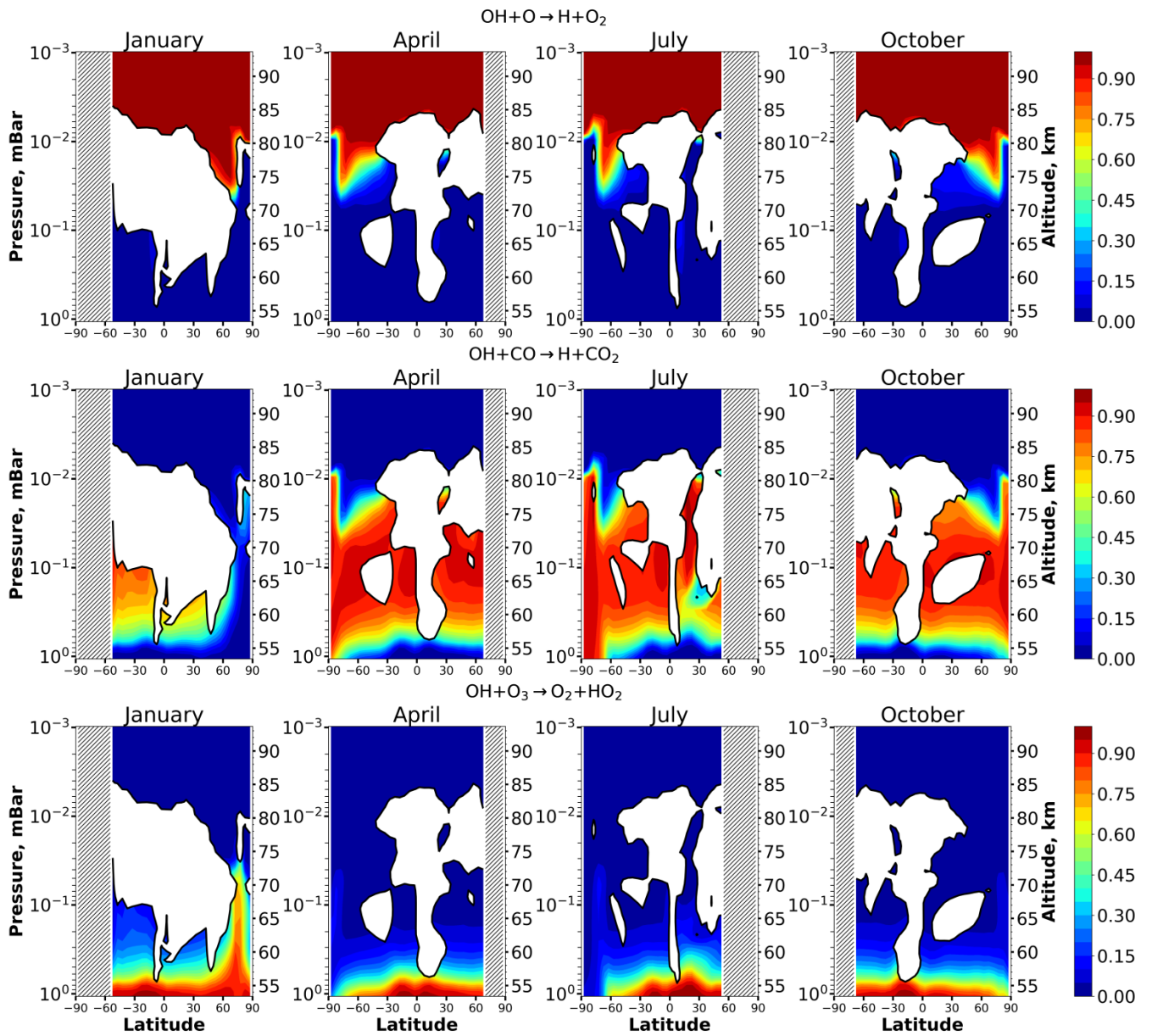


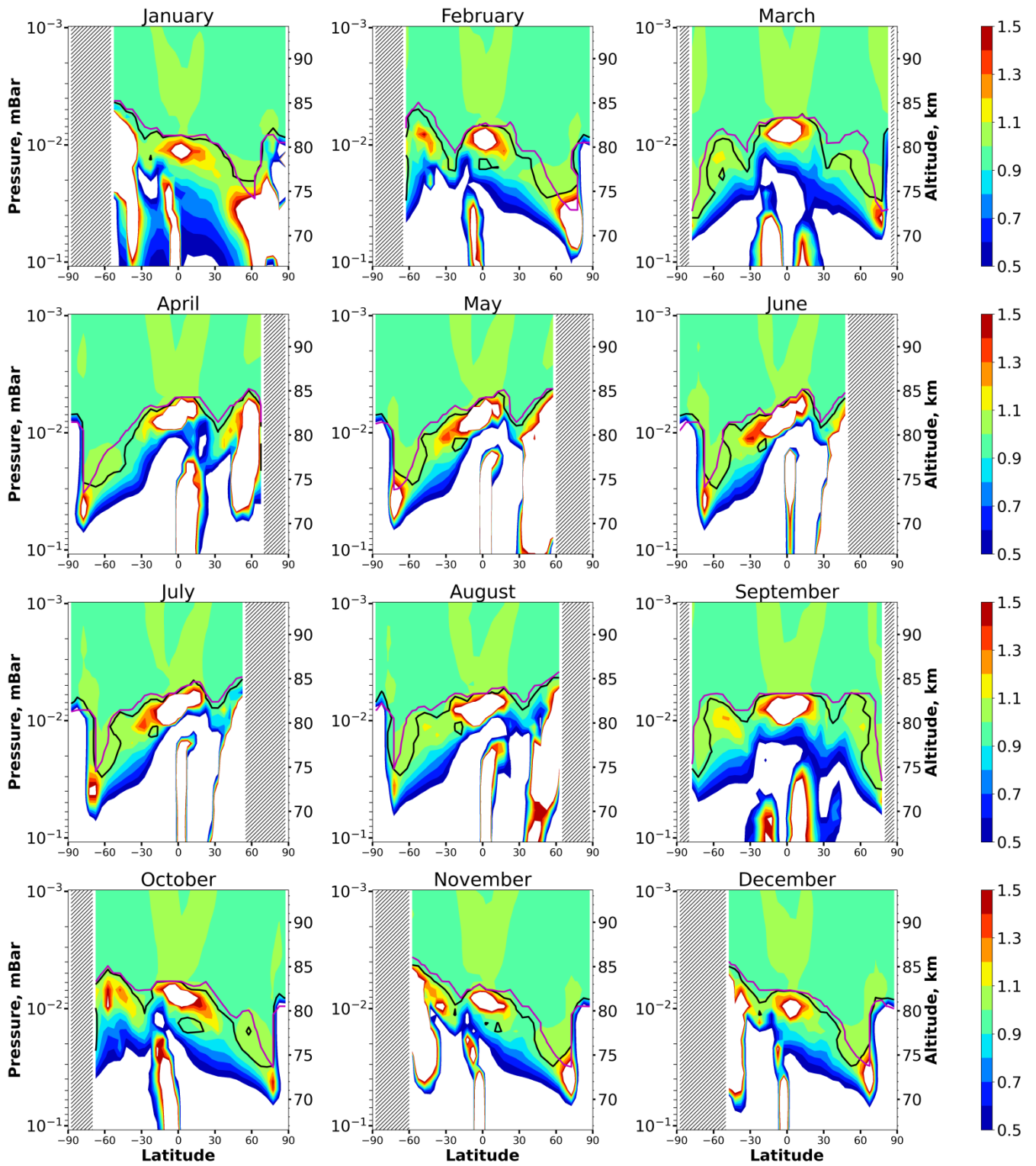
814  
815  
816  
817

Figure 5. Nighttime mean and monthly averaged the relative contribution of a certain reaction to the total source of OH in equilibrium areas (first part). White color points nonequilibrium areas of OH.



818  
 819 **Figure 6. Nighttime mean and monthly averaged the** relative contribution of a certain reaction to the total  
 820 source or sink of OH in equilibrium areas ~~(second part)~~. The stippling corresponds to  $\chi < 105^\circ$ . White  
 821 color points indicates nonequilibrium areas of OH.  
 822



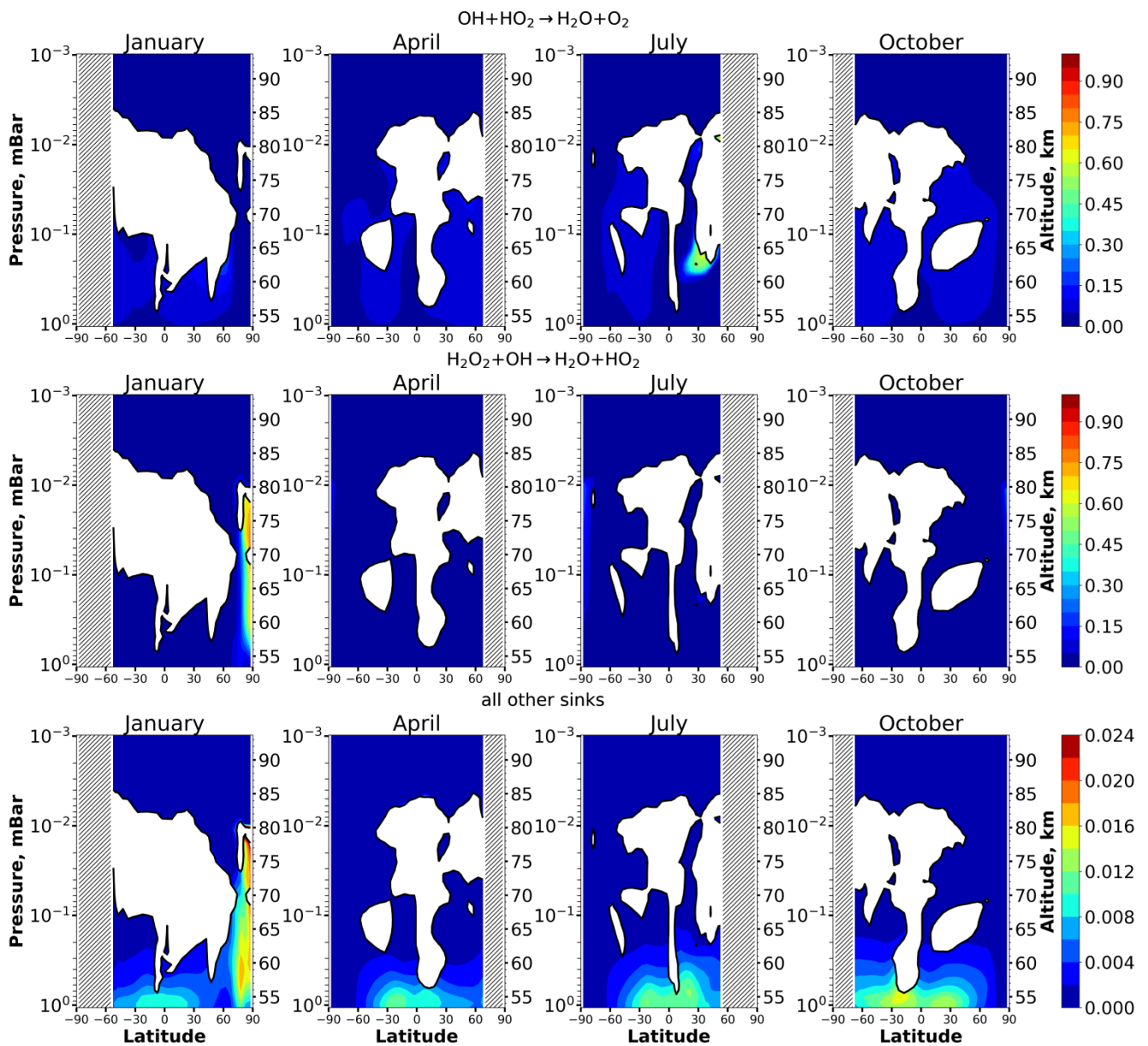


824

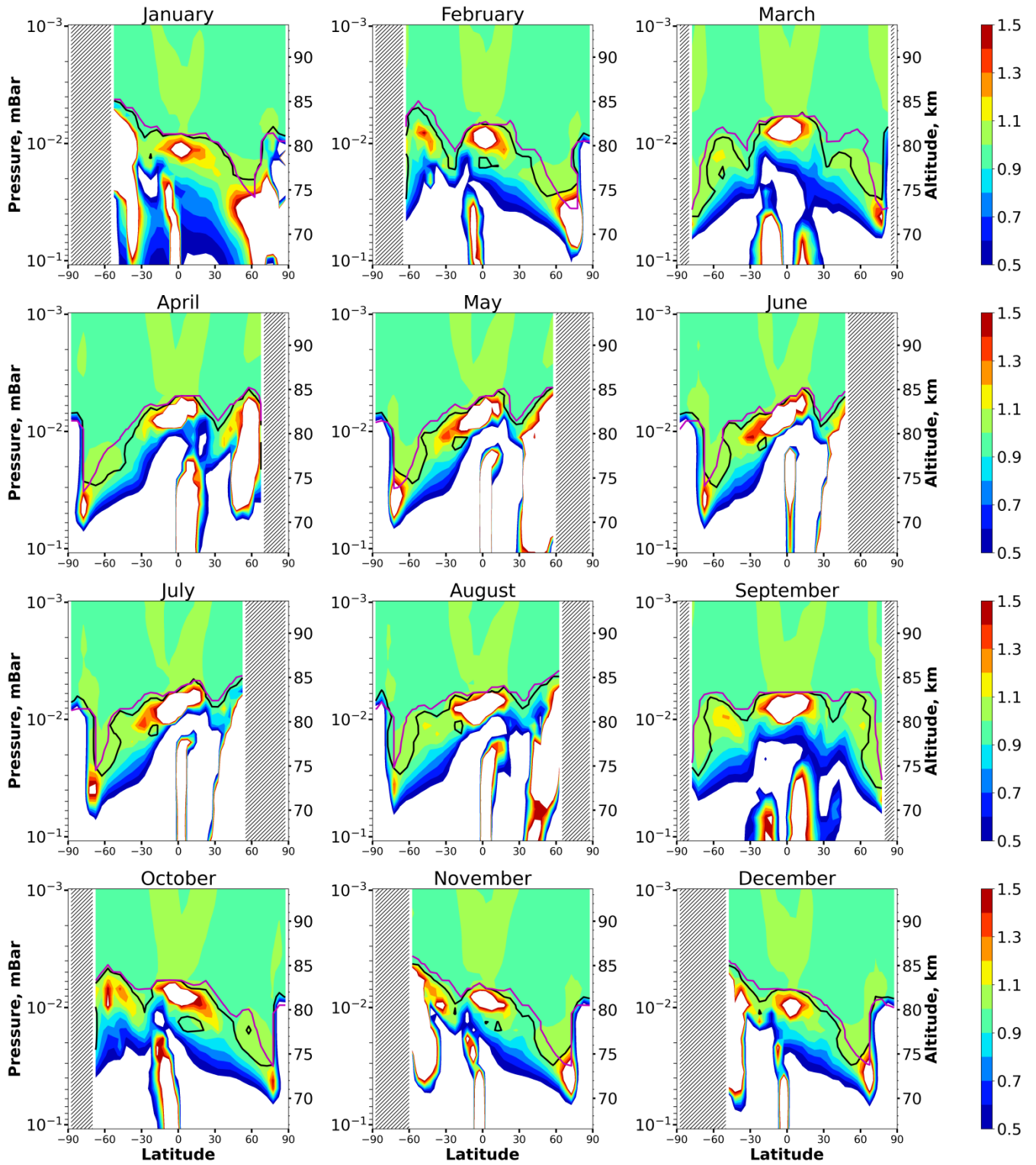
825 Figure 75. Nighttime mean and monthly averaged ~~the relative contribution of a certain reaction to the~~  
 826 ~~total sink of OH in equilibrium areas (first part). White color points nonequilibrium areas of OH.~~

827

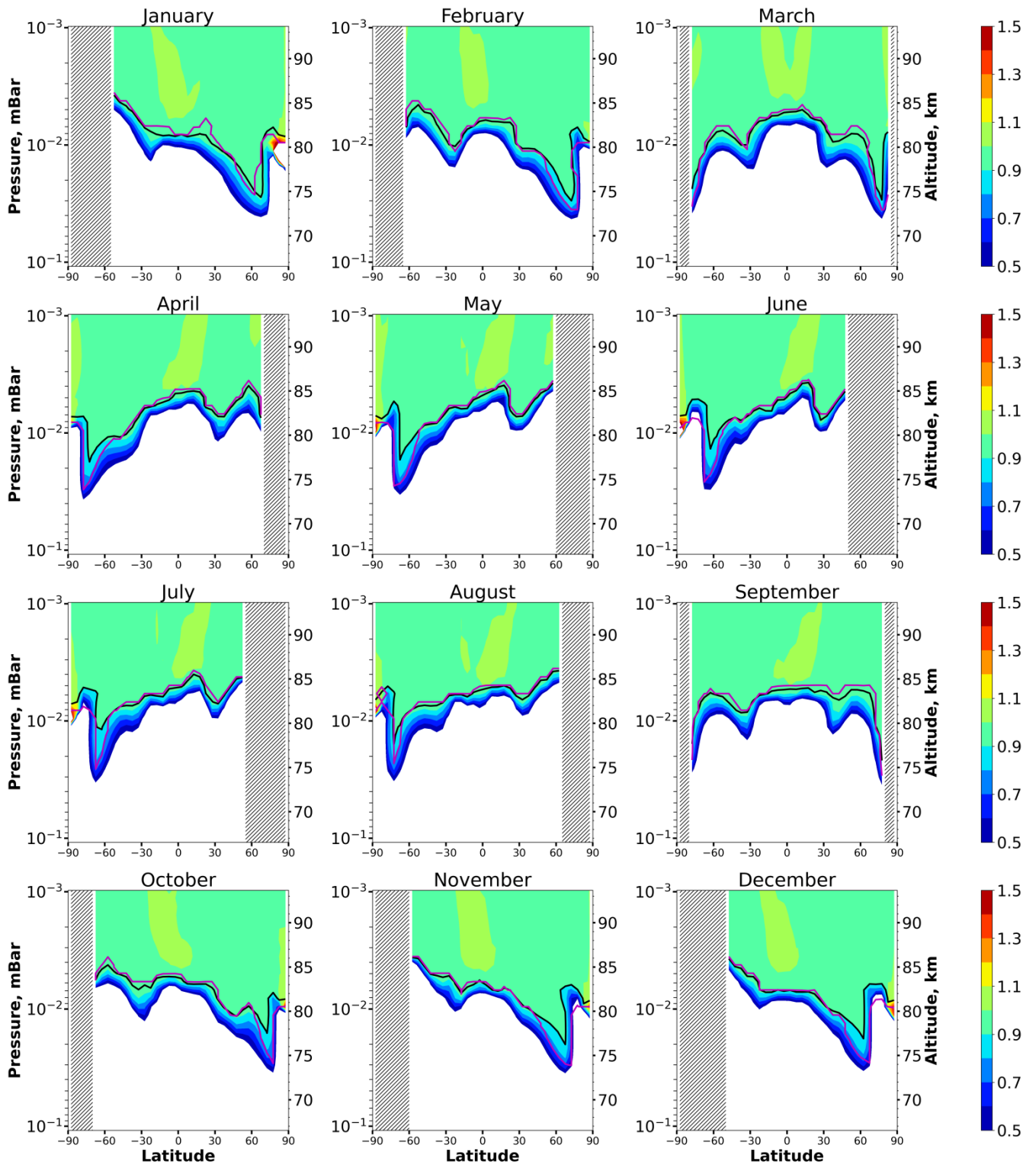
828



829  
 830 **Figure 8. Nighttime mean and monthly averaged the relative contribution of a certain reaction to the total**  
 831 **source of OH in equilibrium areas (second part). White color points nonequilibrium areas of OH.**  
 832



833  
 834 Figure 9. Nighttime mean and monthly averaged  $HO_2/HO_2^{eq}_{sh}$ , where  $HO_2^{eq}_{sh}$  is shortened equilibrium  
 835 concentration determined by Eq. (9). Black line shows the ~~border~~boundary of  $HO_2$  equilibrium according  
 836 to condition (1). Magenta line shows  $\langle Crit_{HO_2} \rangle = 0.1$ . The stippling corresponds to  $\chi < 10^\circ$ . The white  
 837 area represents the  $\langle HO_2/HO_2^{eq} \rangle$  ratio outside the [0.5, 1.5] interval.  
 838

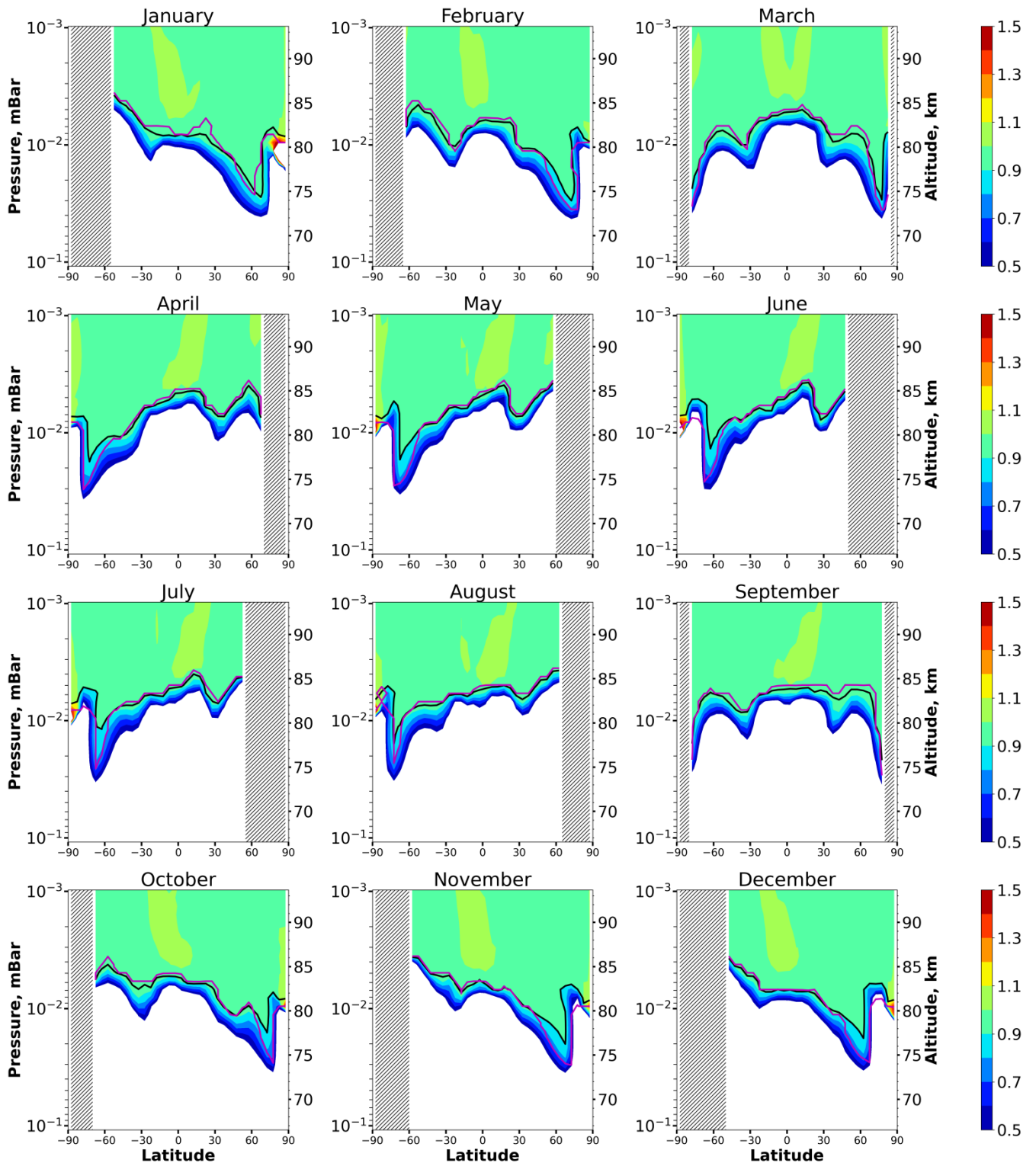


839

840

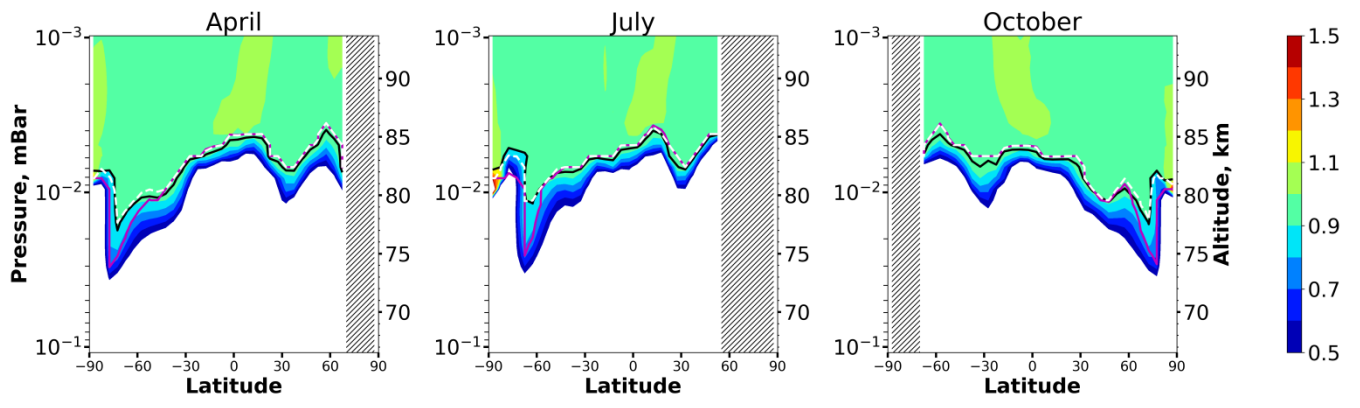
Figure



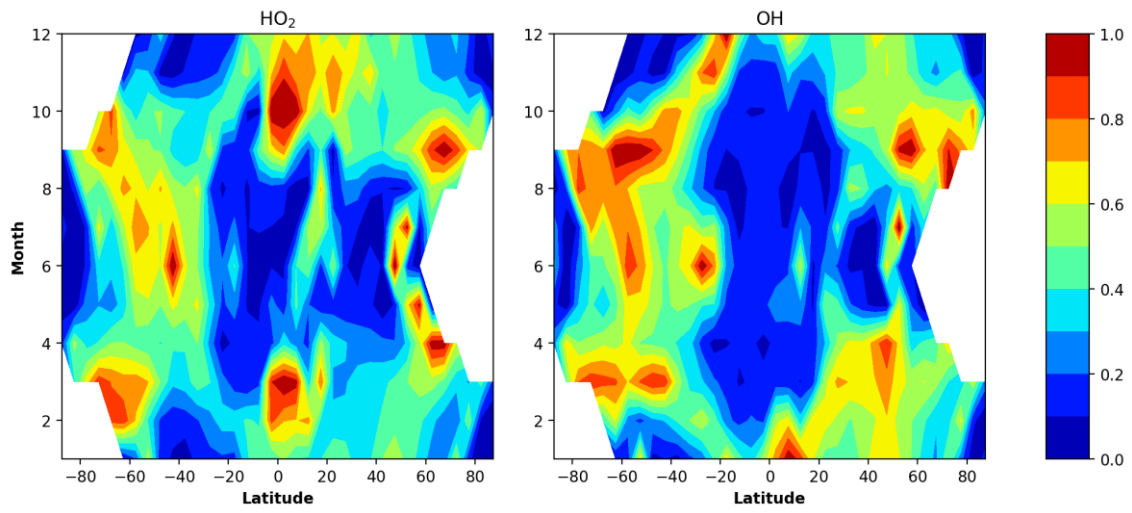


841

842 Figure 6. Nighttime mean and monthly averaged  $OH/OH_{sh}^{eq}$ , where  $OH_{sh}^{eq}$  is shortened equilibrium  
 843 concentration determined by Eq. (10. Nighttime mean and monthly averaged  $OH/OH_{sh}^{eq}$ ). Black line  
 844 shows the border boundary of OH equilibrium according to condition (1). Magenta line shows  $<$   
 845  $Crit_{OH} >= 0.1$ . The stippling corresponds to  $\chi < 105^\circ$ . The white area represents the  $< OH/OH^{eq} >$  ratio  
 846 outside the [0.5, 1.5] interval.



847  
848



849

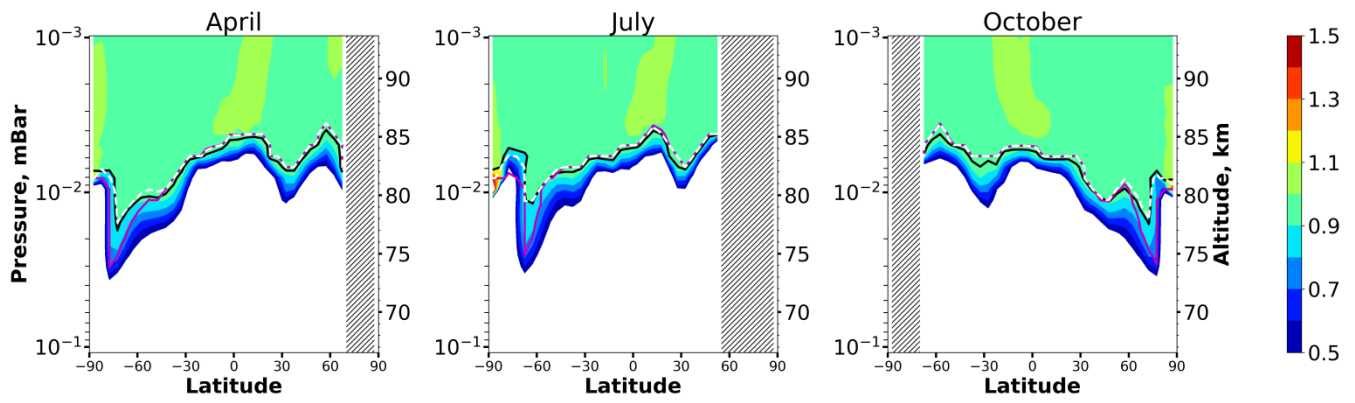
850

851

852

853

Figure 47. Monthly and longitudinally mean of total uncertainties in determination of the local heights of the OH and HO<sub>2</sub> equilibrium boundaries according to the criteria (17) and (25). The white color indicates the absence of data due to polar day.

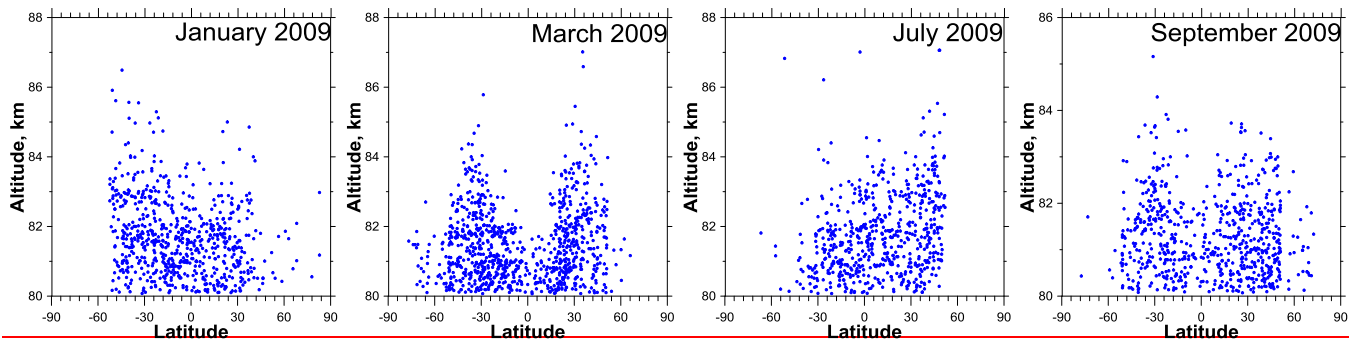


854

855 **Figure 8.** Nighttime mean and monthly averaged  $OH/OH_{sh}^{eq}$ . Black line shows the **borderboundary** of OH  
 856 equilibrium according to condition (1). Magenta line shows  $\langle Crit_{OH} \rangle = 0.1$ , dotted white line shows  
 857  $\langle Crit_{OH}^m \rangle = 0.1$ .

858

859



860  
861 The Figure 12. Blue dots point the found values of  $z_{OH}^{eq}$  above 80 km derived from the Panka et al. data  
862 in different months of 2009.